TU Delft

Delft University of Technology

Influence of high content crumb rubber and different preparation methods on properties of asphalt under different aging conditions

Chemical properties, rheological properties, and fatigue performance

Wang, Sheng; Huang, Weidong; Liu, Xueyan; Lin, Peng

DOI
10.1016/j.conbuildmat.2022.126937

Publication date
2022

Document Version
Final published version

Published in
Construction and Building Materials

Citation (APA)
Wang, S., Huang, W., Liu, X., & Lin, P. (2022). Influence of high content crumb rubber and different preparation methods on properties of asphalt under different aging conditions: Chemical properties, rheological properties, and fatigue performance. *Construction and Building Materials*, *327*, Article 126937. https://doi.org/10.1016/j.conbuildmat.2022.126937

Important note
To cite this publication, please use the final published version (if applicable).
Please check the document version above.

Copyright
Other than for strictly personal use, it is not permitted to download, forward or distribute the text or part of it, without the consent of the author(s) and/or copyright holder(s), unless the work is under an open content license such as Creative Commons.

Takedown policy
Please contact us and provide details if you believe this document breaches copyrights.
We will remove access to the work immediately and investigate your claim.

This work is downloaded from Delft University of Technology.
For technical reasons the number of authors shown on this cover page is limited to a maximum of 10.

Construction and Building Materials 327 (2022) 126937

Contents lists available at ScienceDirect

Construction and Building Materials

journal homepage: www.elsevier.com/locate/conbuildmat

Influence of high content crumb rubber and different preparation methods on properties of asphalt under different aging conditions: Chemical properties, rheological properties, and fatigue performance

Sheng Wang [a], Weidong Huang [a], Xueyan Liu [b], Peng Lin [b,*]

[a] Key Laboratory of Road and Traffic Engineering of Ministry of Education, Tongji University, Tongda Building 4800 Cao'an Road, Shanghai 201804, China
[b] Section of Pavement Engineering, Department of Engineering Structures, Faculty of Civil Engineering and Geosciences, Delft University of Technology, Stevinweg 1, 2628 CN Delft, the Netherlands

ARTICLE INFO

Keywords:
High content crumb rubber modified asphalt
Aging behaviors
ATR-FTIR
Low temperature performance
Fatigue resistance

ABSTRACT

Asphalt pavements are prone to aging in construction and during service, which can affect the properties of the asphalt. The aging behaviors of high content crumb rubber modified asphalt (HCRMA) were investigated in this paper. The binders were aged in the laboratory and the performances before and after aging were tested using the attenuated total reflection-Fourier transform infrared spectroscopy (ATR-FTIR) test, temperature sweep (TS) test, frequency sweep tests, multiple stress creep recovery (MSCR) test, zero shear viscosity (ZSV) test, bending beam rheometer (BBR) test, and linear amplitude sweep (LAS) test. The FTIR test result shows that as the aging progresses, the crumb rubber (CR) continues to undergo desulphurization and degradation reactions in the HCRMA, with the release of substances such as silica and S-C bonded material from the CR into the bituminous phase. The elasticity of HCRMA decreases and then increases as the degree of aging increases. Besides, the low temperature performance of HCRMA is controlled by the stiffness value, and the low temperature stress relaxation properties of HCRMA in the aging process are better than that of 20% content crumb rubber modified asphalt. Moreover, aging can reduce the integrity and fatigue resistance of HCRMA while increasing the compatibility of HCRMA.

1. Introduction

The rapid development of China's automobile industry has led to China becoming a major tire-producing and consuming country. The waste tires of automobiles are not easy to decompose and could produce 'black pollution', which brings huge environmental problems and is also a huge waste of resources [1–4]. The waste crumb rubber (CR) prepared from waste tires as an additive into the asphalt to formulate a crumb rubber modified asphalt (CRMA), not only can effectively solve the environmental problems caused by waste tires, but also improve the properties of binders, thereby improving the properties of asphalt pavement [5–8]. The carbon black and sulphur contained in the CR improve the high temperature stability of the binders [9]. The addition of CR to asphalt improves pavement life and vehicle comfort while reducing road noise [10]. However, the existing method of preparing conventional CRMA is to add CR to asphalt, and then shear at high speed, resulting in most of the CR only swelling and other physical reactions, and CR and asphalt did not form a system, affecting the performance of CRMA and limiting the amount of CR, so that the amount of CR in CRMA is mostly about 20% [11].

Activation treatment and terminal blend process can be used to improve the treatment method of CR content. The activation treatment method of CR is to improve the storage stability of CRMA by changing the physicochemical properties of CR through chemical, physical, mechanical, and biological treatment methods [6]. The fatigue and aging resistance of the CRMA prepared by using ultrasonic treatment of the CR were significantly improved [12]. Ibrahim et al. used the activation method of CR by radiation and determined the corresponding activation parameters [13]. The test results showed that the activated CRMA had good low temperature cracking resistance. Mull et al. found that chemical treatment of the CR increased the solubility of the CR in asphalt and improved the fatigue cracking resistance of the activated

* Corresponding author at: Section of Pavement Engineering, Department of Engineering Structures, Faculty of Civil Engineering and Geosciences, Delft University of Technology, cStevinweg 1, 2628 CN Delft, the Netherlands.
E-mail addresses: shengwang985@163.com (S. Wang), hwd@tongji.edu.cn (W. Huang), X.Liu@tudelft.nl (X. Liu), p.lin-2@tudelft.nl (P. Lin).

https://doi.org/10.1016/j.conbuildmat.2022.126937
Received 10 October 2021; Received in revised form 27 November 2021; Accepted 19 February 2022
Available online 25 February 2022
0950-0618/© 2022 The Authors. Published by Elsevier Ltd. This is an open access article under the CC BY license (http://creativecommons.org/licenses/by/4.0/).

Table 1
Calculation methods of CAI and PAI.

Aging indexes	Calculation methods
CAI	$CAI = G^*_{aged}/ G^*_{unaged}$
PAI	$PAI = \delta_{aged}/ \delta_{unaged}$

Table 2
The methods of calculation of I_{CA}, I_{SU}, I_{S-C}, $I_{Si-O-Si}$, and I_{PB}.

Index	Calculation method
I_{CA}	$I_{CA} = A_{1700\ cm^{-1}}/ A_{1376\ cm^{-1}}$
I_{SU}	$I_{SU} = A_{1030\ cm^{-1}}/A_{1376\ cm^{-1}}$
I_{S-C}	$I_{S-C} = A_{670\ cm^{-1}}/A_{1376\ cm^{-1}}$
$I_{Si-O-Si}$	$I_{Si-O-Si} = A_{1100\ cm^{-1}}/ A_{1376\ cm^{-1}}$
I_{PB}	$I_{PB} = A_{966\ cm^{-1}}/ A_{1376\ cm^{-1}}$

$A_{(XX)cm^{-1}}$ represents the area of (XX) cm^{-1} peak

CRMA [14]. Cheng et al. used a twin-screw extruder to treat polymeric compatibilizers with the CR and found that the storage stability of the activated CRMA was significantly improved [15]. Szerb et al. used fatty acids and organosilanes to treat the surface of the CR, thus improving the compatibility of the CR with the asphalt and the viscoelasticity [16]. Terminal blend rubberized asphalt (TBRA) is a new type of CRMA, which is prepared from finer CR and the base asphalt using a high temperature curing method [17]. Due to the desulfurization reaction and uniform dispersion of CR in asphalt, the TBRA overcomes the technical defects of easy segregation and high viscosity of traditional CRMA and has excellent low-temperature performance, anti-reflection crack ability, and anti-fatigue performance [18–20].

Compared with CRMA with 20% CR content, high content crumb rubber modified asphalt (HCRMA) (e.g. dosage of around 50%) exhibits advantages. On the one hand, the use of HCRMA can increase the recycling of CR, while reducing the environmental problems caused by waste tires, to save cost to a greater extent. On the other hand, the low temperature performance of asphalt pavement is improved after using HCRMA [21–23]. However, similar to conventional modified asphalt [24,25], as blended organic compound materials, HCRMA binders are subject to aging. The hardening of the neat asphalt and the desulphurization of CR caused by aging weaken the effectiveness of CR, while also leading to coupling reactions between asphalt and CR, resulting in various pavement distresses [26–28]. As a result, the aging of HCRMA remains an issue of great concern, which affects the performance of asphalt.

In this paper, the aging performance of HCRMA with different preparation methods was studied. The attenuated total reflection-Fourier transform infrared spectroscopy (ATR-FTIR) test, temperature sweep (TS) test, frequency sweep tests, multiple stress creep recovery (MSCR) test, zero shear viscosity (ZSV) test, bending beam rheometer (BBR) test, and linear amplitude sweep (LAS) test are conducted to evaluate the chemical properties, rutting resistance, rheological properties, low temperature performance, fatigue resistance, and

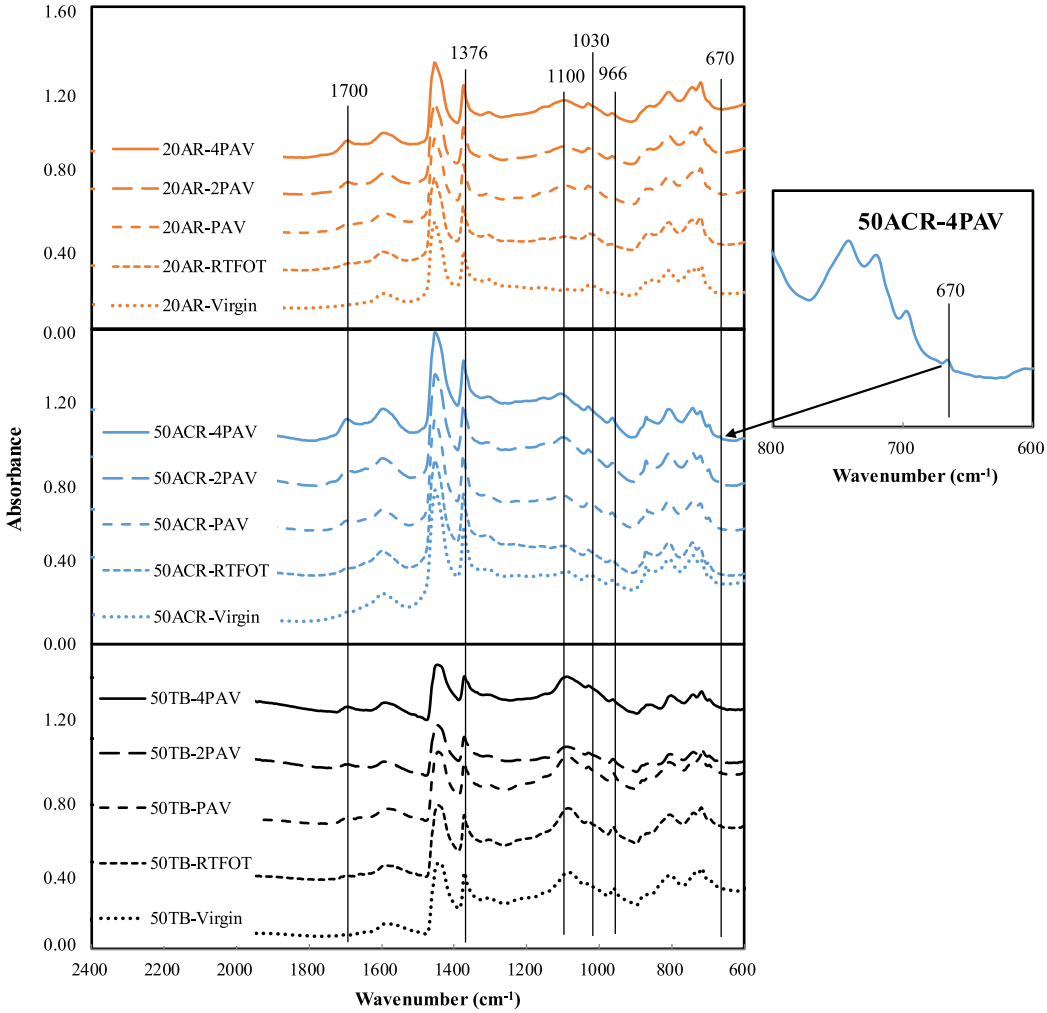

Fig. 1. ATR-FTIR spectra of 20AR, 50ACR, and 50 TB before and after aging.

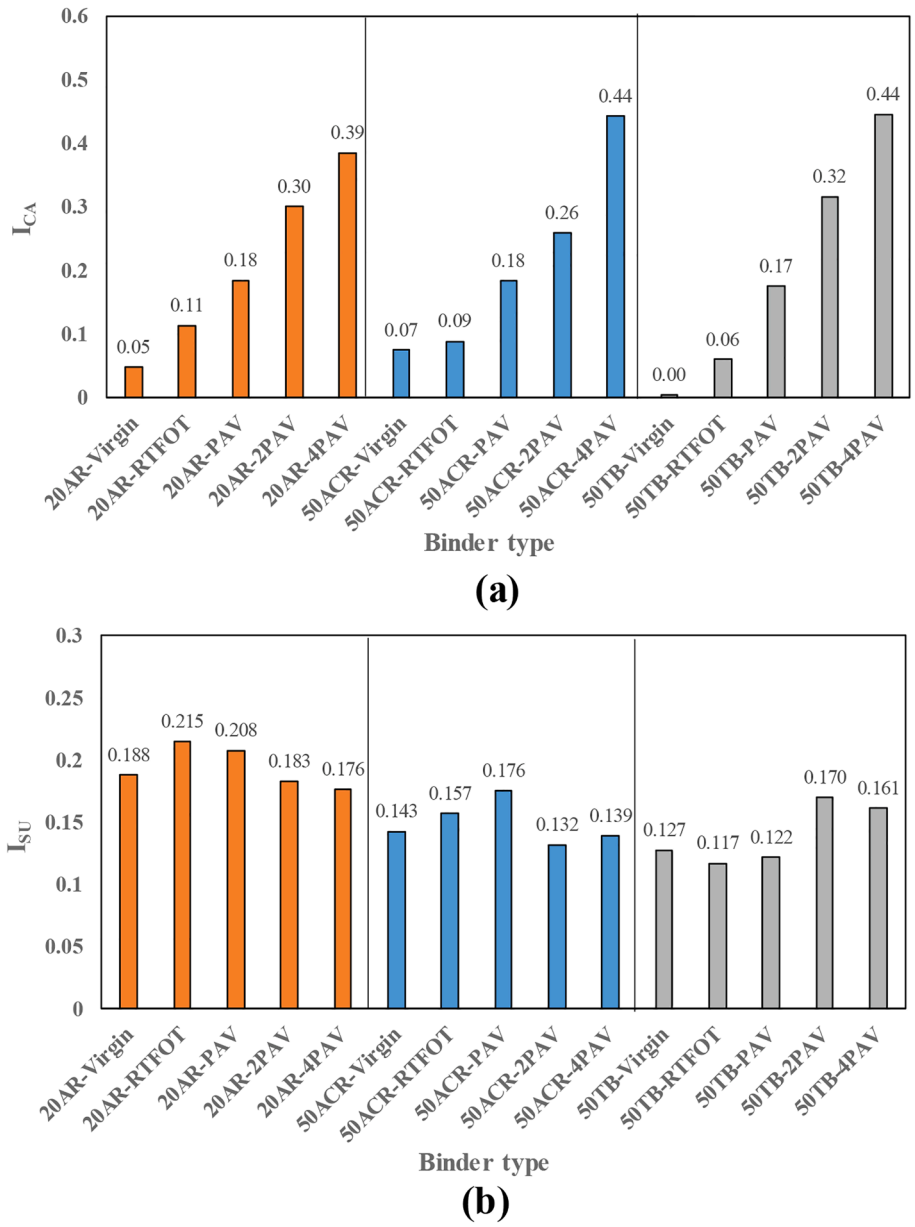

Fig. 2. I_{CA} and I_{SU} of 20AR, 50ACR, and 50 TB before and after aging: (a) I_{CA}, (b) I_{SU}.

compatibility of HCRMA before and after aging, respectively. Besides, the anti-aging properties of HCRMA were evaluated by the complex modulus aging index (CAI) and phase angle aging index (PAI).

2. Material and methods

2.1. Materials

There are two kinds of HCRMA, namely activated crumb rubber modified asphalt (ACRMA) and TBRA in this paper. The finished ACRMA with the content of CR of 50% (wt.), was from Hebei Jingde Expressway Co., Ltd, China. The conventional properties of ACRMA such as ductility (5 °C), softening point, penetration (25 °C), and rotational viscosity (180℃) are 18.9 cm, 78.2 °C, 42 dmm, and 2.89 Pa·s, respectively. ACRMA is prepared by adding CR and activator to the neat asphalt (PG 64–16) at 180 °C for 50 min at 2000 rpm [21]. The TBRA was made of CR (50% by weight of TBRA) and neat asphalt (PG 64–16). The minus 30 mesh CR, containing 54% natural rubber and synthesis rubber was produced in Jiangyin, China. Referring to the high temperature curing method of previous studies [17,20], TBRA was prepared by adding CR to the neat asphalt and mixing in a sealed tank at 260 °C for 6 h with a stirring speed of 400 rpm to ensure adequate degradation of the CR. To compare the performance of the HCRMA, a 20% content crumb rubber modified asphalt was prepared, which was made by heating the neat asphalt to 180℃ and then adding the CR and mixing for 1.5 h. For convenience, 20% content crumb rubber modified asphalt, ACRMA, and TBRA used in this article were named 20AR, 50ACR, and 50 TB respectively.

2.2. Aging procedures

Accordance with AASHTO M 320–14 [29], rolling thin film oven aging (RTFOT), 20 h of standard pressure aging vessel (PAV), 40 h of PAV aging, and 80 h of PAV aging were carried out on the 20AR, 50ACR, and 50 TB, respectively. For convenience, three PAV aging conditions used in this paper were named PAV, 2PAV, and 4PAV respectively. The aging resistance of 20AR, 50ACR, and 50 TB was evaluated using the complex modulus aging index (CAI) and phase angle aging index (PAI),

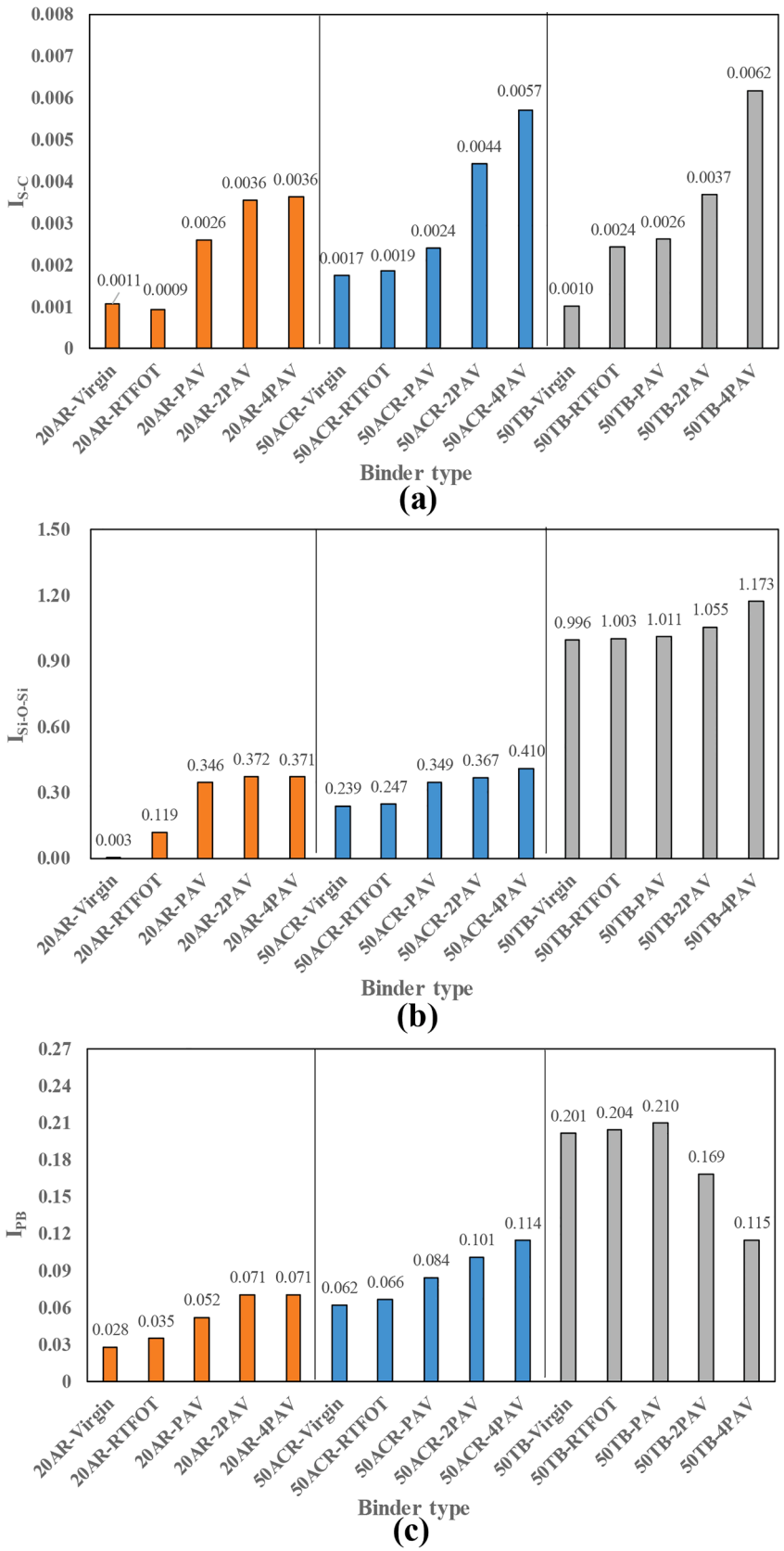

Fig. 3. I_{S-C}, $I_{Si-O-Si}$, and I_{PB} of 20AR, 50ACR, and 50 TB before and after aging: (a) I_{S-C}, (b) $I_{Si-O-Si}$, and, (c) I_{PB}.

Table 3
ΔI_{CA} of 20AR, 50ACR, and 50 TB before and after aging.

Sample	20AR		50ACR		50 TB	
	I_{CA}	ΔI_{CA}	I_{CA}	ΔI_{CA}	I_{CA}	ΔI_{CA}
Unaged	0.048	–	0.075	–	0.004	–
RTFOT aging	0.114	0.066	0.089	0.014	0.060	0.056
PAV aging	0.184	0.136	0.183	0.109	0.175	0.171
2PAV aging	0.300	0.252	0.259	0.184	0.316	0.312
4PAV aging	0.385	0.337	0.442	0.368	0.445	0.440

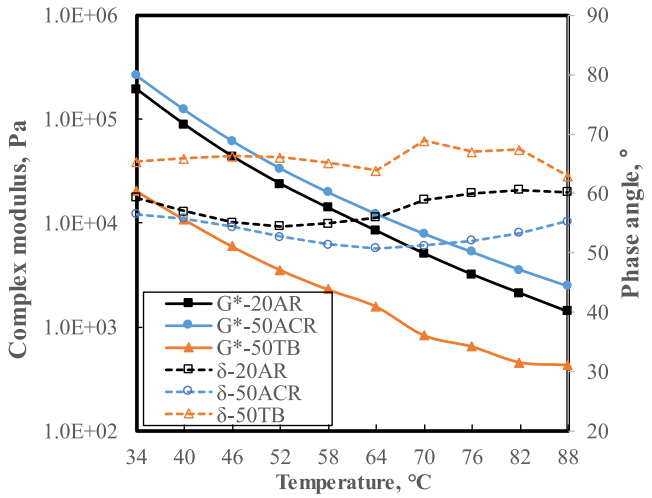

Fig. 4. G* and δ of 20AR, 50ACR, and 50 TB.

which are calculated in Table 1 [30,31].

2.3. ATR-FTIR test

In this paper, 20AR, 50ACR, and 50 TB before and after aging were covered on the surface of the ATR reflector crystal and fixed with a metal laminate so that asphalt was in full contact with the ATR diamond, and the binders were subjected to 32 scans in the wavenumber range of 4000–600 cm^{-1}. The spectra obtained from the scans were analyzed by means of the OMNIC software. Five infrared characteristic indexes, namely carbonyl index (I_{CA}), sulfoxide index (I_{SU}), I_{S-C}, silica index ($I_{Si-O-Si}$), and polybutadiene index (I_{PB}), were obtained by analysis, which was used to quantify the oxidation degree of HCRMA and the desulfurization level of CR respectively. Carbonyl and sulfoxide are two common oxidation functional groups. Therefore, the I_{CA} and the I_{SU} were chosen to evaluate the oxidation levels of 20AR, 50ACR, and 50 TB in this study [31]. In addition, when the CR in asphalt is subjected to aging, it undergoes a desulphurization and degradation reaction, allowing some of the S-C cross-linked bonds and silica to enter the asphalt phase [17]. Some scholars also define I_{PB} index to characterize the desulfurization degree of CR [32]. In this paper, I_{S-C}, $I_{Si-O-Si}$, and I_{PB} were selected for quantitative analysis and comparison of desulfurization degree in 20AR, 50ACR, and 50 TB before and after aging. Higher values of I_{S-C}, $I_{Si-O-Si}$, and I_{PB} indicate greater desulphurization of the HCRMA. The calculation methods of I_{CA}, I_{SU}, I_{S-C}, $I_{Si-O-Si}$, and I_{PB} were presented in Table 2.

2.4. Rheological properties tests

2.4.1. Temperature sweep (TS) test and master curves

In accordance with AASHTO M 320–14 [29], dynamic shear rheometer (DSR) was performed to obtain the storage modulus (G′), loss modulus (G″), complex modulus (G*) and phase angle (δ) of the 20AR, 50ACR, and 50 TB before and after aging in the range of 34℃ to 88℃ with an increment of 6℃. In this paper, master curves for G*, δ, G′, and G″ were constructed from frequency sweep tests on 20AR, 50ACR, and 50 TB before and after aging at 5℃, 15℃, 25℃, 35℃, 45℃, 55℃, 65℃ and 75℃. The test frequencies were set between 0.1 and 30 Hz. The sigmoidal model and the time–temperature superposition principle (TTSP) were used to construct the master curves of G*, δ, G′, and G″, using 25 °C as the reference temperature for the fit. The specific steps have been described in a previous paper [33]. Han curves [34] of 20AR, 50ACR, and 50 TB before and after aging were calculated by temperature scanning and frequency scanning data respectively.

2.4.2. Multiple stress creep recovery (MSCR) test and zero shear viscosity (ZSV) test

The MSCR tests were performed on the 20AR, 50ACR, and 50 TB before and after aging at 64℃, 70℃, 76℃, and 82℃, according to AASHTO M 332–14 [35]. The zero shear viscosity (ZSV) of asphalt is the viscosity value of asphalt at an infinite shear rate close to zero, which is an index to evaluate the high temperature performance of the binder. ZSV values were obtained by fitting a Carreau model to steady-state shear test data at 60 °C for 20AR, 50ACR, and 50 TB before and after

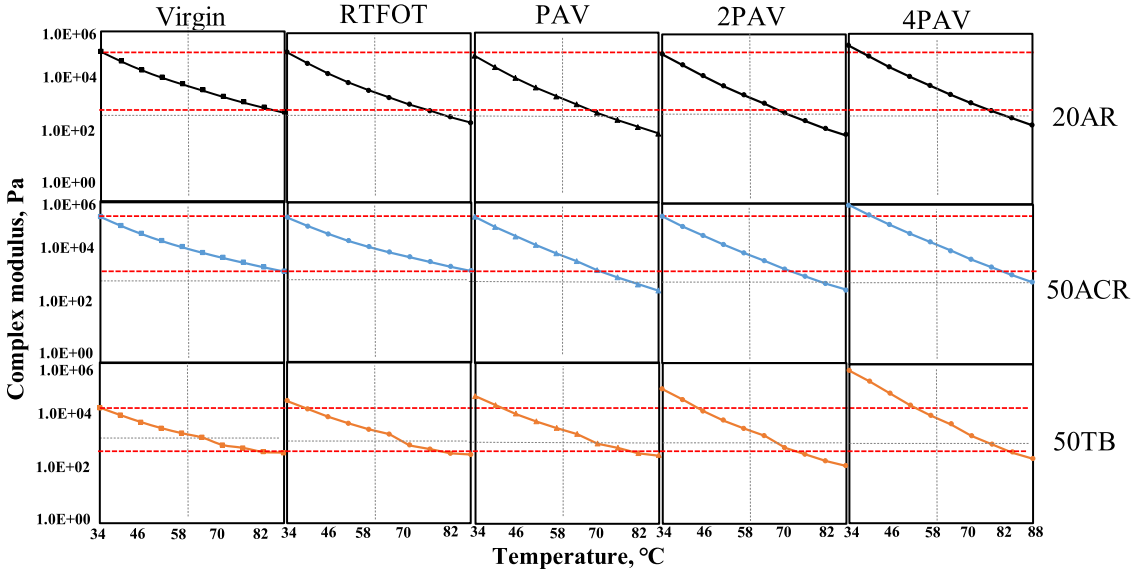

Fig. 5. G* evolution of 20AR, 50ACR, and 50 TB along with aging.

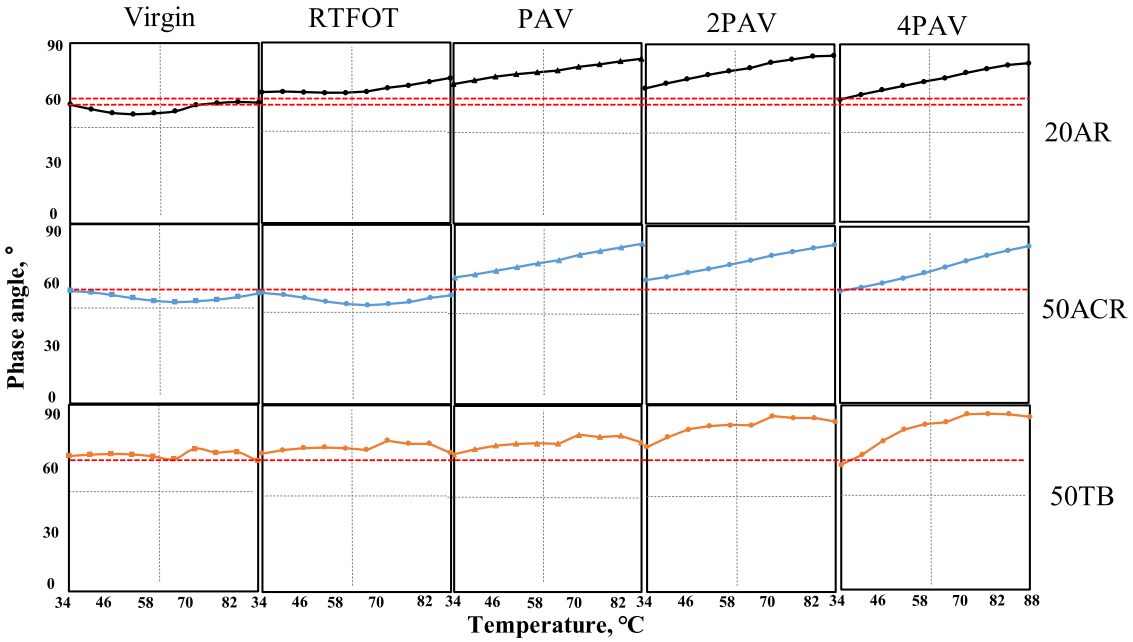

Fig. 6. δ evolution of 20AR, 50ACR, and 50 TB along with aging.

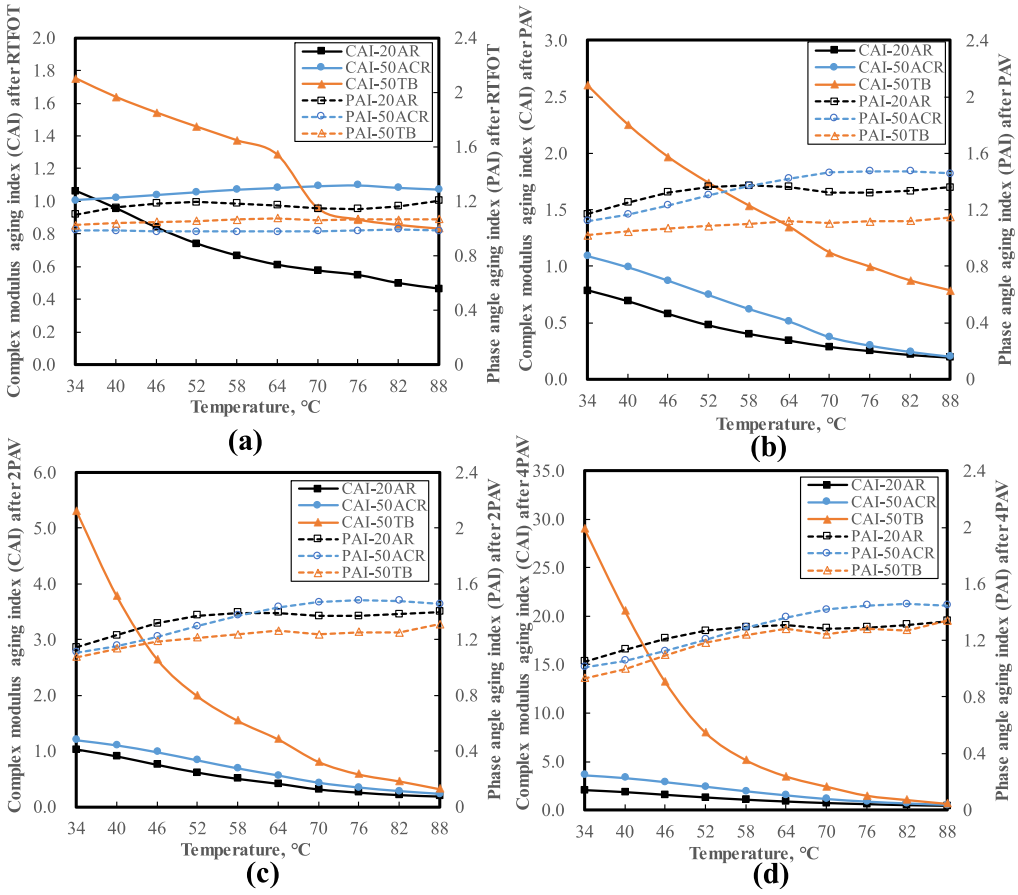

Fig. 7. CAI and PAI of 20AR, 50ACR, and 50 TB: (a) RTFOT, (b) PAV, (c) 2PAV, (d) 4PAV.

aging in this study. The shear rate of the steady-state shear test is 0.01 s^{-1} to 100 s^{-1}.

2.4.3. *Bending beam rheometer (BBR) test*

The stiffness (S) and the creep rate (m-value) of the 20AR, 50ACR, and 50 TB after PAV aging were measured using the BBR test at −12℃,

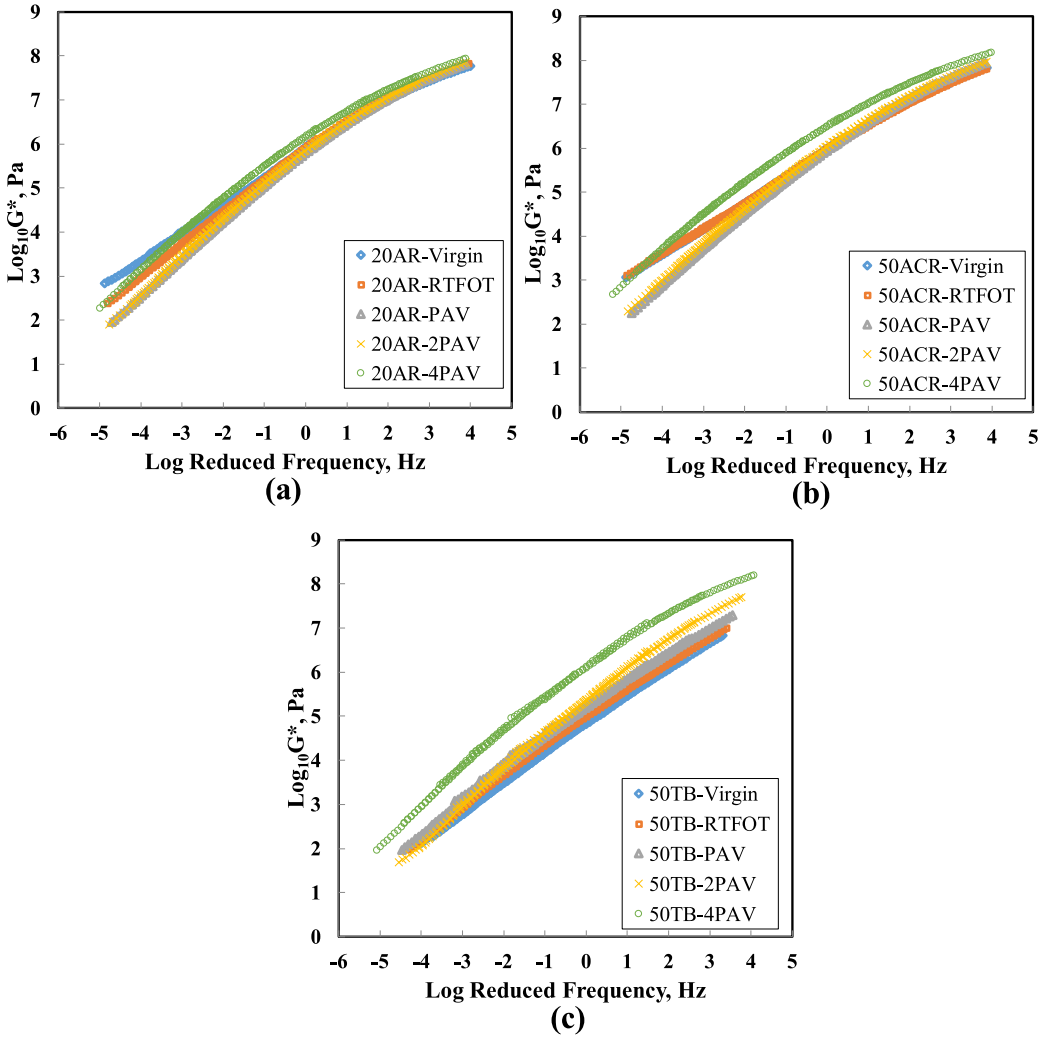

Fig. 8. G* master curves of 20AR, 50ACR, and 50 TB: (a) 20AR, (b)50ACR, (c) 50 TB.

−18℃, −24℃, and −30℃ according to the low temperature evaluation method of ASTM D6648 [36]. Tsp and Tmp represent the PG low temperature at an S value of 300 MPa and an m-value of 0.3 for the PAV aging condition, respectively. The PG low temperature grade for asphalt is the higher value of Tsp and Tmp [37,38]. The difference between Tsp and Tmp is adopted to study the low temperature performance of HCRMA and named ΔT. The Δ T value>0 indicates that the stress relaxation performance of the binder is controlled by S, and ΔT<0 indicates that the stress relaxation performance of the binder is controlled by m-value [38]. The calculation method for ΔT is described below:

$$\Delta T = Tsp - Tmp \quad (1)$$

2.4.4. Linear amplitude sweep (LAS) test and fatigue factor

The fatigue performance of the 20AR, 50ACR, and 50 TB was assessed at 25 °C using the LAS test according to AASHTO TP101 [39–42]. Also, the fatigue factor (G*·sin δ) of the 20AR, 50ACR, and 50 TB was measured with DSR at 25 °C and a fixed frequency of 10 rad/s.

3. Results and discussion

3.1. ATR-FTIR analysis

The FTIR spectra of 20AR, 50ACR, and 50 TB at various aging conditions are shown in Fig. 1 and homologous I_{CA}, I_{SU}, $I_{S\text{-}C}$, $I_{Si\text{-}O\text{-}Si}$, and I_{PB} are presented in Fig. 2 and Fig. 3. From Fig. 2, the I_{CA} increases for the same HCRMA from RTFOT to 4PAV aging, but the I_{SU} of HCRMA does not become larger with increasing aging. The reason for this phenomenon is that the products of asphalt oxidation are mainly carbonyl and sulfoxide, but sulfoxide is unstable at high temperatures, and deep aging may cause the degradation of sulfoxide. Therefore, compared with I_{SU}, the I_{CA} is more recommended as a chemical index to judge the oxidation degree of HCRMA. To quantitatively analyze the anti-oxidation ability of HCRMA, ΔI_{CA} is used, which is the value of the difference of I_{CA} between virgin and aged HCRMA [31], and ΔI_{CA} values are shown in Table 3. According to Table 3, under the 4PAV aging method, the ΔI_{CA} ranking is 20AR < 50ACR < 50 TB, indicating that compared with 20AR and 50ACR, 50 TB exhibits the lowest anti-oxidation ability at 4PAV aging condition.

Fig. 3 (a) and Fig. 3(b) show that $I_{S\text{-}C}$ and $I_{Si\text{-}O\text{-}Si}$ of the HCRMA increase from virgin condition to 4PAV aging condition, indicating that as the aging progresses, the CR continues to undergo desulphurization and degradation reactions, with the release of substances such as silica and S-C bonded material from the CR into the bituminous phase. Moreover, the $I_{Si\text{-}O\text{-}Si}$ of the 50 TB is higher than that of the 20AR and 50 TB at virgin condition. This is because 50 TB in its unaged state has a higher degree of desulphurization than 50ACR and 20AR. Meanwhile, according to Fig. 3(c), the I_{PB} increases with aging for 20AR and 50ACR, while the opposite result is obtained for 50 TB. The reason for this phenomenon is

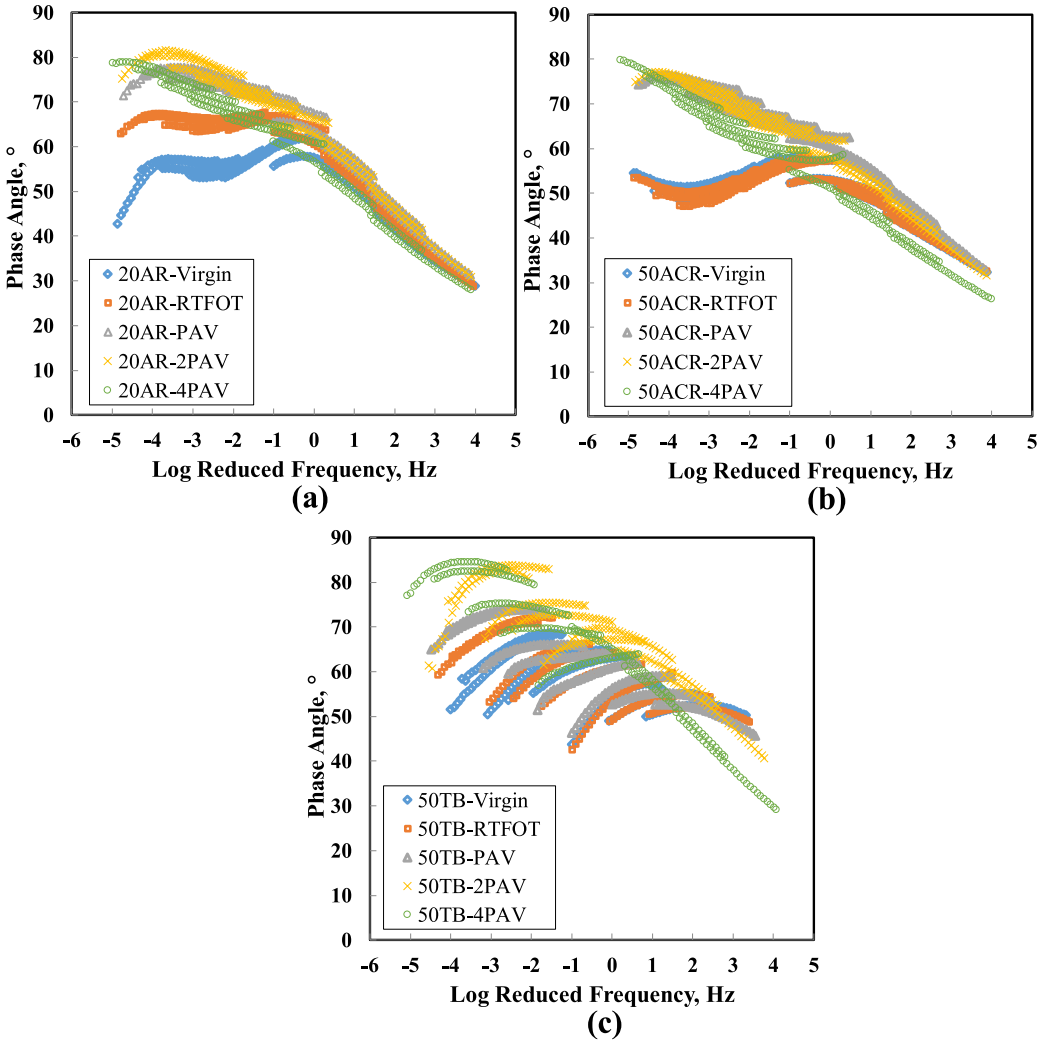

Fig. 9. δ master curves of 20AR, 50ACR, and 50 TB: (a) 20AR, (b)50ACR, (c) 50 TB.

that compared with 20AR and 50ACR, the polybutadiene polymer in 50 TB degrades under deep aging, resulting in the decrease of I_{PB} value. Therefore, $I_{S\text{-}C}$ and $I_{Si\text{-}O\text{-}Si}$ are more recommended than I_{PB} as chemical indicators for judging the degree of HCRMA desulphurization.

3.2. TS test result analysis

3.2.1. Evaluation of G* and δ

The changes of G* and δ of 20AR, 50ACR, and 50 TB at unaged conditions are shown in Fig. 4. The order of G* of the HCRMA is 50 TB < 20AR < 50ACR. The G* value of 50ACR is bigger than that of the 20AR and 50 TB. In addition, the ranking of δ values is 50ACR < 20AR < 50 TB, which shows that the δ ranking is the opposite of that of G*. This is mainly due to the increased swelling reaction of the CR as the amount of CR is increased, resulting in a higher asphaltene concentration in 50ACR and the natural rubber in the CR also has a beneficial influence on the performance of the asphalt, resulting in an improvement in the high temperature property of 50ACR. In addition, the desulphurization and full degradation of the CR in 50 TB causes it to lose some of its rubber elasticity, resulting in a reduction in its high temperature rutting resistance [11].

To study the evolution of G* and δ of 20AR, 50ACR, and 50 TB with the aging degree, the G* curves and δ curves are sorted in terms of types of 20AR, 50ACR, and 50 TB and shown in Fig. 5 and Fig. 6. As shown in Fig. 5, the G* of 20AR and 50ACR shows a decreasing trend with aging and 50 TB changes with aging in the opposite order to 20AR and 50ACR. As described in Fig. 6, the δ values of 20AR, 50ACR, and 50 TB increase from virgin state to 4PAV. This shows that the viscous components of 20AR, 50ACR, and 50 TB increase with aging, which is caused by CR desulfurization and polymer degradation in 20AR, 50ACR, and 50 TB.

3.2.2. Aging resistance

Fig. 7 shows the CAI and PAI of 20AR, 50ACR, and 50 TB after RTFOT, PAV, 2PAV, and 4PAV, respectively. By comparing among 20AR, 50ACR, and 50 TB after RTFOT, PAV, 2PAV, and 4PAV, the all rankings of CAI values after RTFOT, PAV, 2PAV, and 4PAV aging is 20AR < 50ACR < 50 TB. In addition, the ranking of PAI is 50ACR < 50 TB < 20AR after RTFOT and the ranking of PAI is 50 TB < 50ACR < 20AR from 34 to 58℃ after PAV, 2PAV, and 4PAV aging. The above results show that 20AR has better anti-aging properties than 50 TB and 50ACR through rheological aging index evaluation. On the one hand, after AR20 has undergone aging, the degradation of CR desulphurization deepens, resulting in a certain degree of destruction of the network structure and loss of rubber properties, which slows down the hardening effect of aging on AR20 and plays a role in improving the anti-aging properties. On the other hand, with the increase of CR content in HCRMA, the contact area between CR and oxygen is smaller, which reduces the degree of desulphurization and degradation of CR, resulting

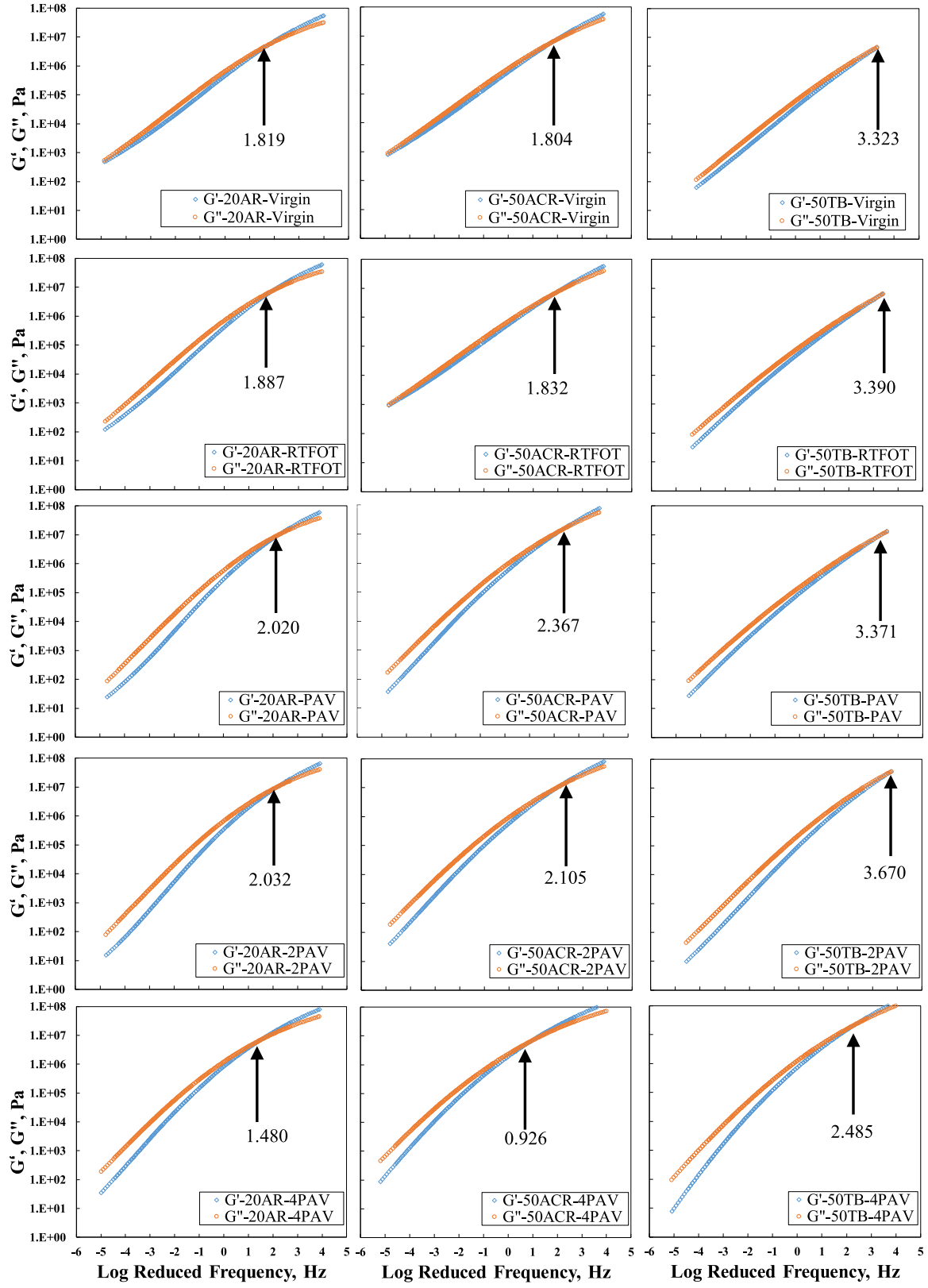

Fig. 10. Evolution of the master curves of G' and G'' of 20AR, 50ACR, and 50 TB with aging.

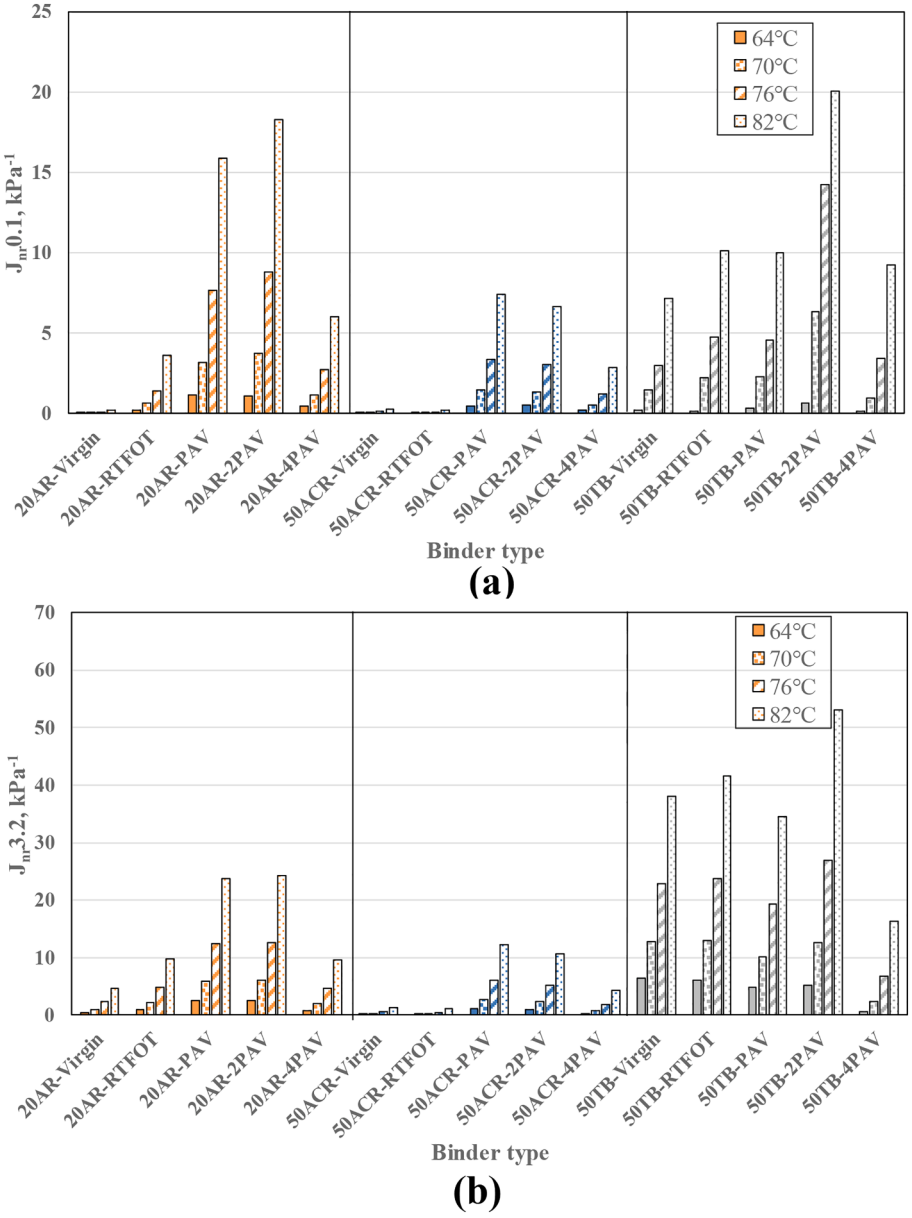

Fig. 11. J_{nr} of 20AR, 50ACR, and 50 TB before and after aging: (a) $J_{nr}0.1$; (b) $J_{nr}3.2$.

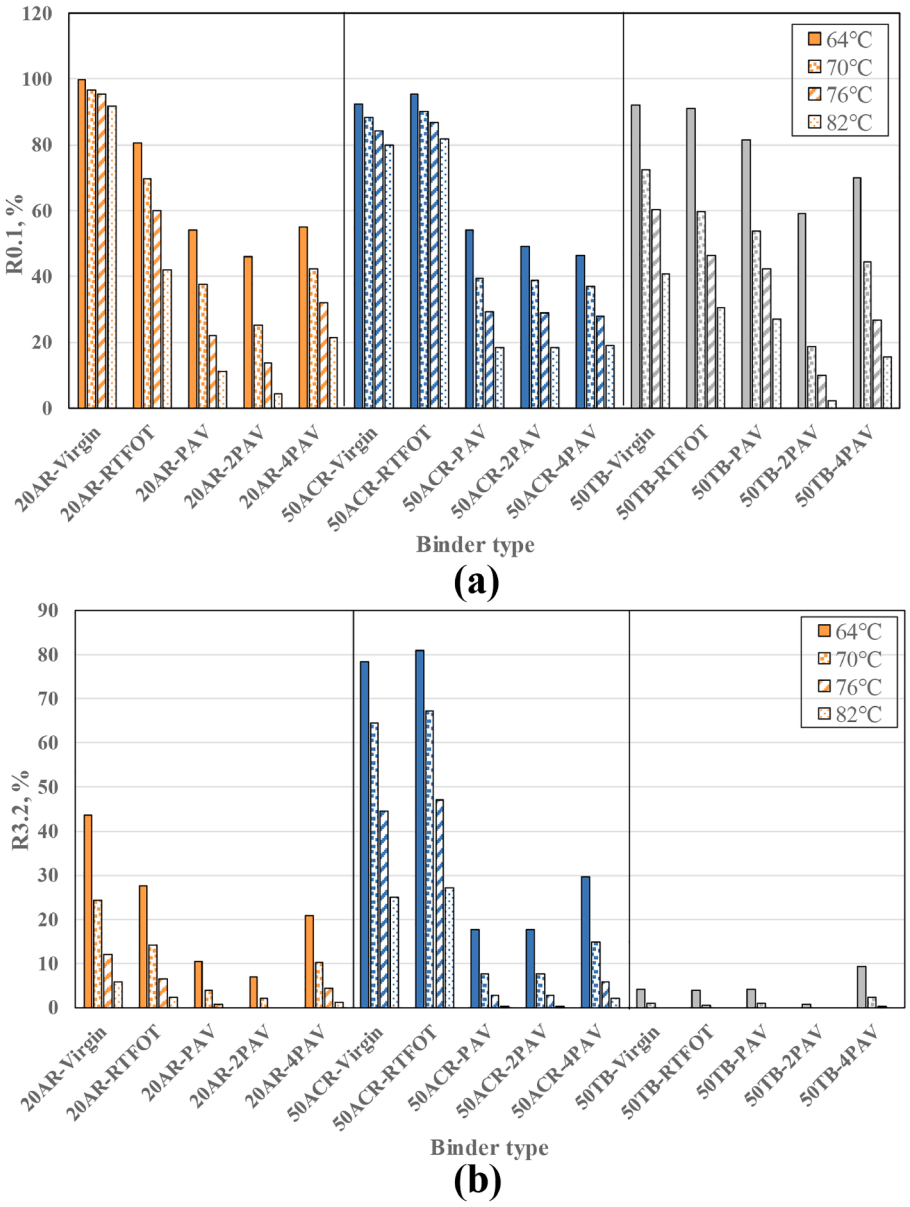

Fig. 12. R of 20AR, 50ACR, and 50 TB before and after aging: (a) R0.1; (b) R3.2.

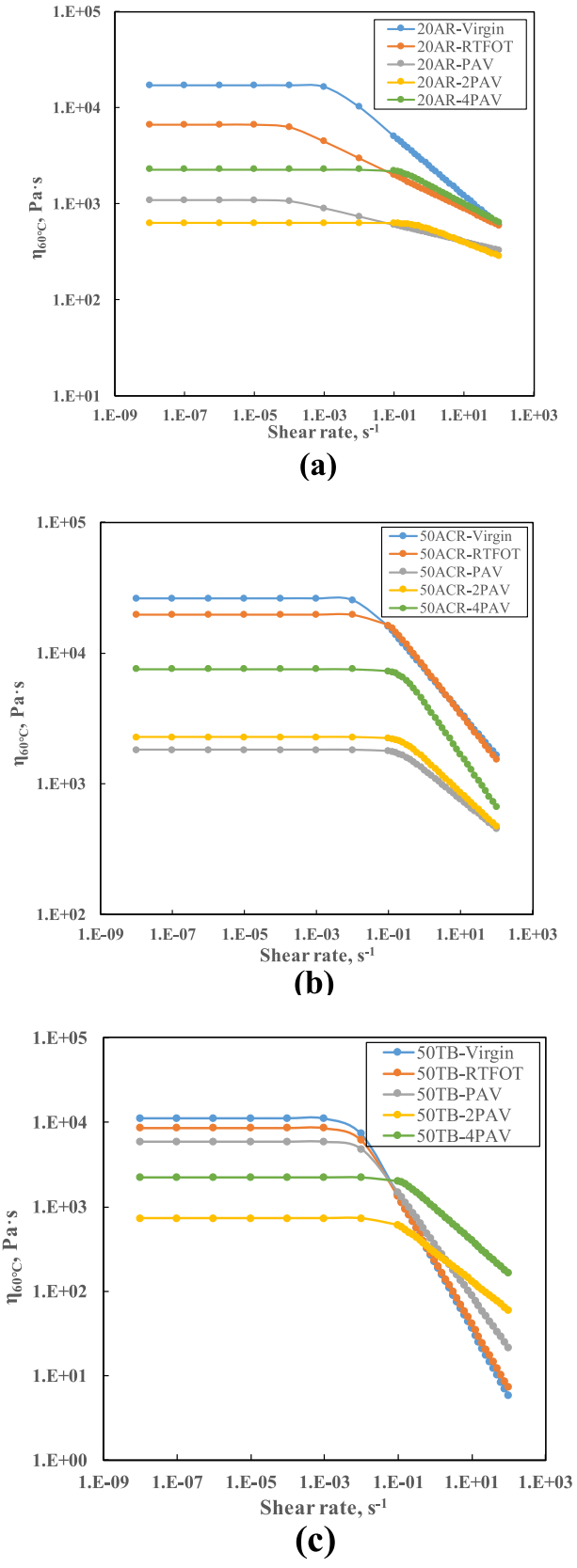

Fig. 13. ZSV curves of 20AR, 50ACR, and 50 TB before and after aging at 60 °C: (a) 20AR; (b) 50ACR; (c) 50 TB.

Table 4
ZSV of 20AR, 50ACR, and 50 TB before and after aging at 60 °C.

Sample Name	ZSV at 60 ℃, Pa·s				
	Virgin	RTFOT	PAV	2PAV	4PAV
20AR	17123.73	6681.60	1097.17	627.66	2278.08
50ACR	26333.23	19723.73	1819.11	2285.34	7551.87
50 TB	11226.83	8644.48	5849.27	729.40	2251.25

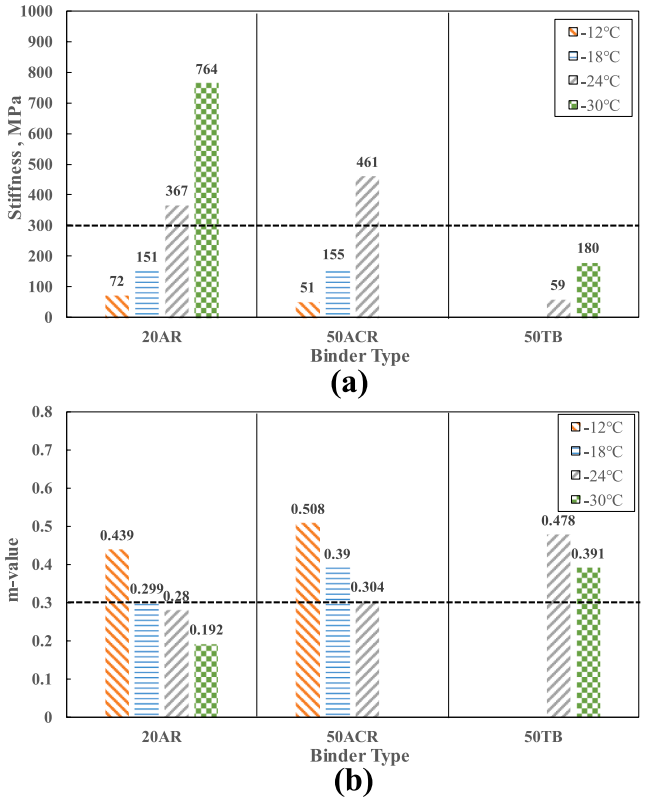

Fig. 14. Stiffness and m-value of 20AR, 50ACR, and 50 TB at PAV aging condition: (a) Stiffness; (b) m-value.

Table 5
PG low temperature results of 20AR, 50ACR, and 50 TB.

Sample Name	Tsp (S = 300 MPa), ℃	T_{mp} (m = 0.3), ℃	ΔT, ℃	PG, ℃
20AR	−33.0	−28.5	−4.5	−28.5
50ACR	−31.6	−34.3	2.7	−31.6
50 TB	−42.8	−47.5	4.7	−42.8

in a higher CAI and smaller PAI of HCRMA.

3.3. Master curves result analysis

Fig. 8 and Fig. 9 show the G* master curves and δ master curves of 20AR, 50ACR, and 50 TB at various aging conditions. As shown in Fig. 8 (a), 20AR has the biggest complex modulus master curves at 4PAV condition. In the high frequency region, aging has little effect on the master curve of G* of AR20. Based on Fig. 8(b), the complex modulus master curves of 50ACR are higher than virgin 50ACR. Besides, in Fig. 8 (c), with more severe aging, the G* master curve of 50 TB increases gradually. The above results show that the G* master curves of HCRMA increases after deep aging. As described in Fig. 9(a), after the aging, the δ master curves of 20AR increase at low frequencies (high temperatures), while the phase angle master curves of 20AR decrease after aging in the high frequency region (low temperature region). The change law of

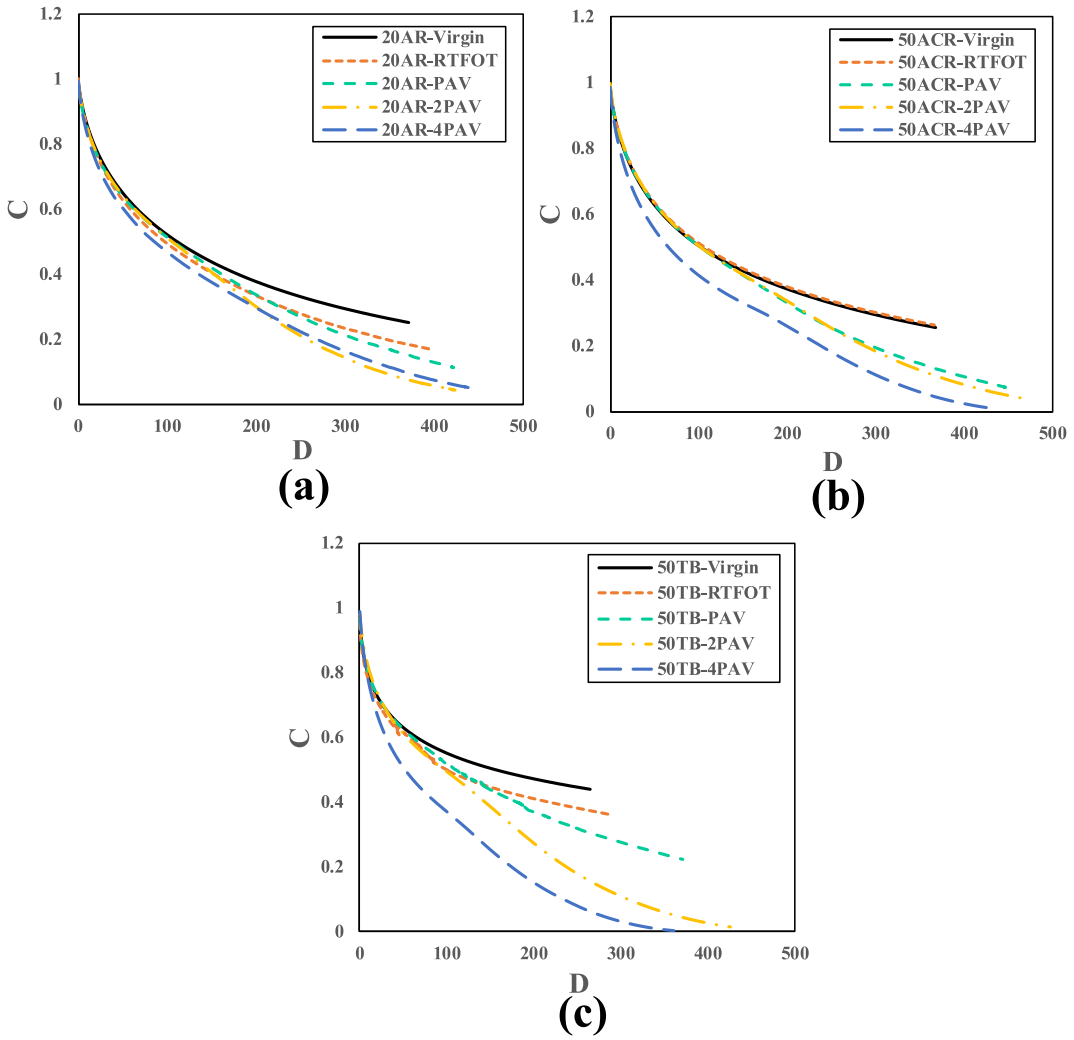

Fig. 15. Damage characteristic curves of 20AR, 50ACR, and 50 TB: (a) 20AR, (b)50ACR, (c) 50 TB.

phase angle master curves of 50ACR and 50 TB after aging is similar to that of 20AR in Fig. 9(b) and Fig. 9(c). This phenomenon is due to the that in the high frequency region (low temperature region), the hardening effect of aging HCRMA leads to a smaller phase angle, and in the low frequency region (high temperature region), the desulphurization of the CR and degradation of the polymer in HCRMA leads to a smaller phase angle [20].

The G′ master curves and G″ master curves of 20AR, 50ACR, and 50 TB before and after aging are presented in Fig. 10. The G′ and G″ of 20AR, 50ACR, and 50 TB increase with increasing frequency. During the temperature increase, the different rates of increase of G′ master curves and G″ master curves lead to an intersection point between G′ master curves and G″ master curves. In the frequency region before this intersection point, G'' is greater than G' and the asphalt exhibits a more viscous component, and in the frequency region after the intersection point, G' and G'' shift in size and G' is greater than G'' leading to a more elastic behavior of the asphalt. The logarithmic frequencies corresponding to the intersection point of 20AR, 50ACR, and 50 TB increase and then decrease as the degree of aging increases, indicating that aging changes the conversion frequency of the elasticity and viscosity of HCRMA by first increasing the conversion frequency intersection (lowering the temperature) and then decreasing the conversion frequency intersection (increasing the temperature) due to the desulphurization and polymer degradation that occurs in HCRMA at the beginning of aging softening the asphalt, leading to an increase in the frequency intersection point, and as the degree of aging increases, the degree of asphalt hardening exceeds the degree of asphalt softening leading to an increase in the conversion frequency intersection point.

3.4. MSCR test result analysis

The recovery (R) and the non-recoverable creep compliance (J_{nr}) were used as evaluation indicators to analyze the high temperature properties of 20AR, 50ACR, and 50 TB under different aging conditions [43]. The R values at the two stress levels of 0.1 kPa and 3.2 kPa were expressed as R0.1 and R3.2, respectively, while J_{nr} at the two stress levels was expressed as $J_{nr}0.1$ and $J_{nr}3.2$, respectively. Fig. 11 provides $J_{nr}0.1$ and $J_{nr}3.2$ of 20AR, 50ACR, and 50 TB before and after aging. Fig. 11 (a) shows that under unaged and RTFOT aged condition, the $J_{nr}0.1$ values of 50 TB at 64℃, 70℃, 76℃, and 82℃ are bigger than that of 20AR, and 50ACR have the lowest $J_{nr}0.1$, illustrating 20AR is less resistant to rutting than the 50ACR. In addition, the 50 TB has the worst rutting resistance. As the degree of aging deepens, the $J_{nr}0.1$ value of HCRMA first increases and then decreases. The regular changes of $J_{nr}0.1$ and $J_{nr}3.2$ after aging are consistent at 64℃, 70℃, 76℃, and 82℃. Fig. 12 shows the R0.1 and R3.2 of 20AR, 50ACR, and 50 TB before and after aging. R0.1 and R3.2 of HCRMA before and after aging follow the same regular change, in contrast to the regularity of J_{nr}, indicating that aging first increases the viscosity of HCRMA, and then improves its elasticity.

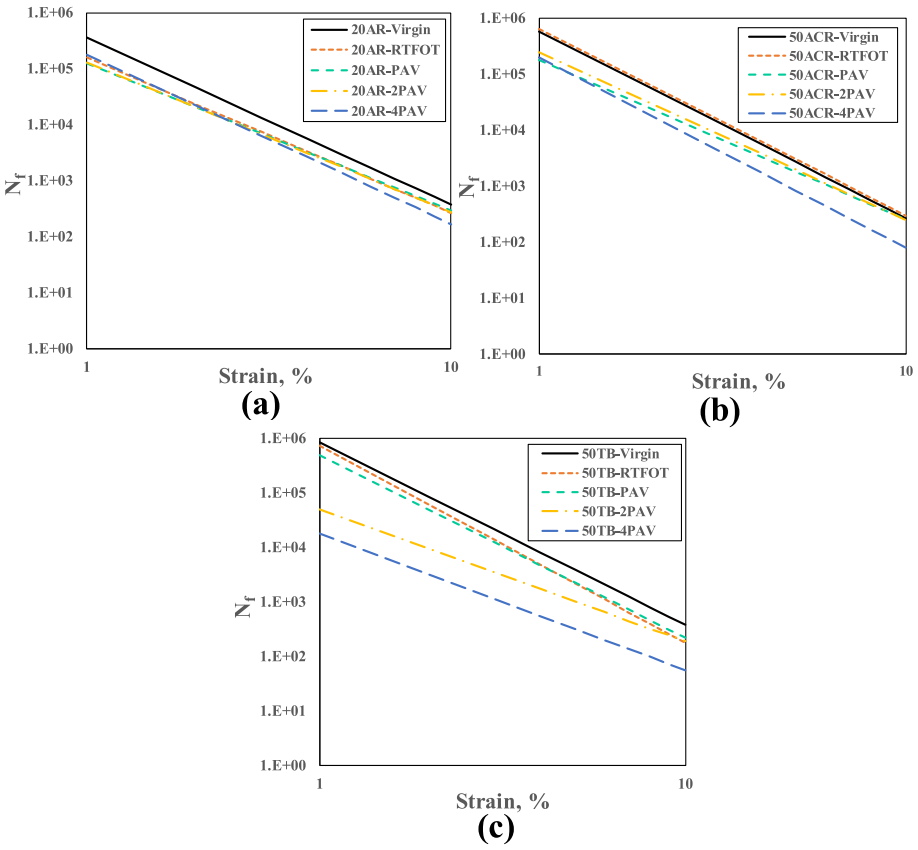

Fig. 16. Fatigue curves of 20AR, 50ACR, and 50 TB: (a) 20AR, (b)50ACR, (c) 50 TB.

3.5. ZSV test result analysis

The ZSV of asphalt is the viscosity value of asphalt at an infinite shear rate close to zero used to evaluate the high temperature properties of binders [44,45]. The higher value of ZSV means that the better rutting resistance of asphalt. The ZSV curves of 20AR, 50ACR, and 50 TB before and after aging are presented in Fig. 13, and the corresponding ZSV at 60℃ is shown in Table 4. As shown in Table 4, the ZSV of 20AR is lower under unaged conditions compared to 50ACR, indicating that the high temperature performance of 20AR is reduced compared to 50ACR. Besides, the ZSV of 50 TB is the lowest at 60 °C. The larger ZSV of 50ACR is due to the high doping of CR, which leads to the absorption of lighter components in the asphalt and the difficulty of moving CR particles, and the presence of vulcanizing agents in CR, which can cross-link the CR molecules into a network structure, increasing the ZSV of 50ACR. The ZSV of 20AR, 50ACR, and 50 TB decreases and then increases with aging due to the desulphurization of the CR and degradation of the polymer in HCRMA [46].

3.6. BBR test result analysis

The changes in stiffness and m-value of 20AR, 50ACR, and 50 TB at PAV aging conditions are shown in Fig. 14. Larger S values and smaller m-values for asphalt indicate poorer stress relaxation properties and greater susceptibility to cracking [18]. Based on Fig. 14(a), the S value for 50ACR at 24℃ increases compared to 20AR, while the S value for 50 TB decreases, and the ranking of S value at 24℃ is 50ACR > 20AR > 50 TB. Besides, the ranking of m-value at 24℃ is 50 TB > 50ACR > 20AR. In other words, the low temperature stress relaxation properties of 50 TB are better than that of 50ACR and 20AR.

PG low temperatures of 20AR, 50ACR, and 50 TB are displayed in Table 5. According to Table 5, the ranking of Δ T is 50 TB > 50ACR > 0 > -2.5 > 20AR > -5 [47,48], and the ranking of PG low temperature value is 20AR > 50ACR > 50 TB. The above results show that the low temperature properties of HCRMA binders are controlled by the S value, and the low temperature crack resistance of 50 TB in the PAV aging process is better than that of 20AR and 50ACR. This is due to the desulphurization and degradation reaction of CR in the process of TB preparation, which leads to the aging resistance, crosslinking agent, and carbon black in CR to enter the asphalt phase, thereby improving the low temperature performance of 50 TB [17,31].

3.7. Fatigue performance analysis

3.7.1. LAS result test

The damage characteristic curves for 20AR, 50ACR, and 50 TB according to the LAS test are shown in Fig. 15. When the integrity parameter (C) is equal to 1, the sample is in an undamaged complete state, and when C is equal to 0, the sample is completely damaged. For a given failure strength (D) value, the larger the C, the stronger the material's ability to resist damage [49]. In accordance with Fig. 15, the C values of 20AR, 50ACR, and 50 TB before aging are higher than that of the 20AR, 50ACR, and 50 TB after aging. The results show that the integrity of HCRMA becomes worse after aging. The fatigue life (N_f) curves for the 20AR, 50ACR, and 50 TB at the different aging conditions predicted by the VECD model are presented in Fig. 16. For comparison purposes, the N_f at 2.5% and 5% strain levels is shown in Fig. 17. Based on Fig. 17, at 2.5% strain, the sequence of N_f of 20AR, 50ACR, and 50 TB is the same as that under 5% strain at the different aging conditions. The ranking of N_f before aging is 50 TB > 50ACR > 20AR, indicating that compared with 20AR and 50ACR, the fatigue resistance of 50 TB before aging is improved. In addition, with more severe aging, the N_f of 20AR, 50ACR, and 50 TB decrease, and the N_f of 50 TB decreases more significantly.

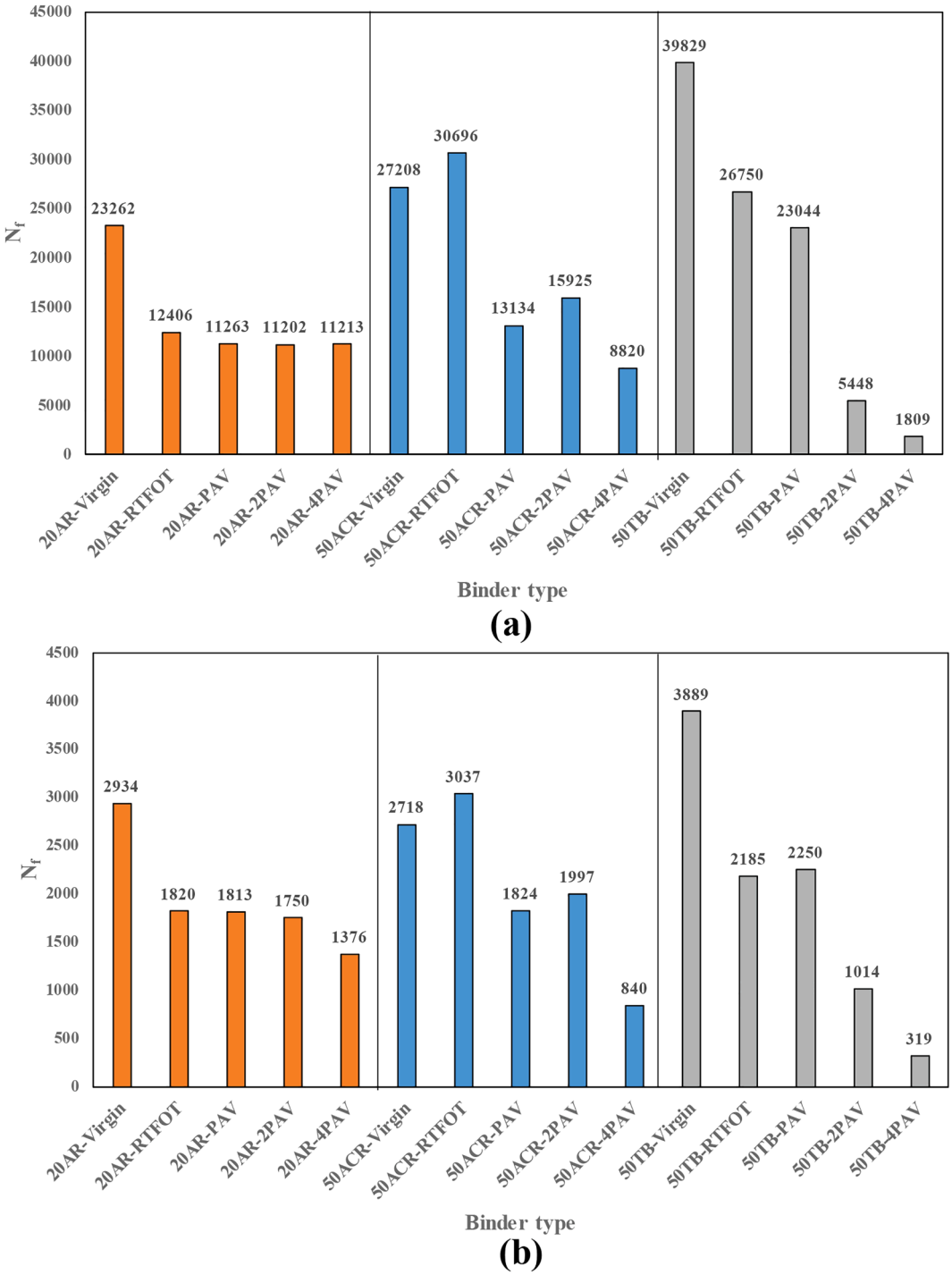

Fig. 17. N_f at different strain levels: (a) N_f of 20AR, 50ACR, and 50 TB at 2.5% strain, (b) N_f of 20AR, 50ACR, and 50 TB at 5% strain.

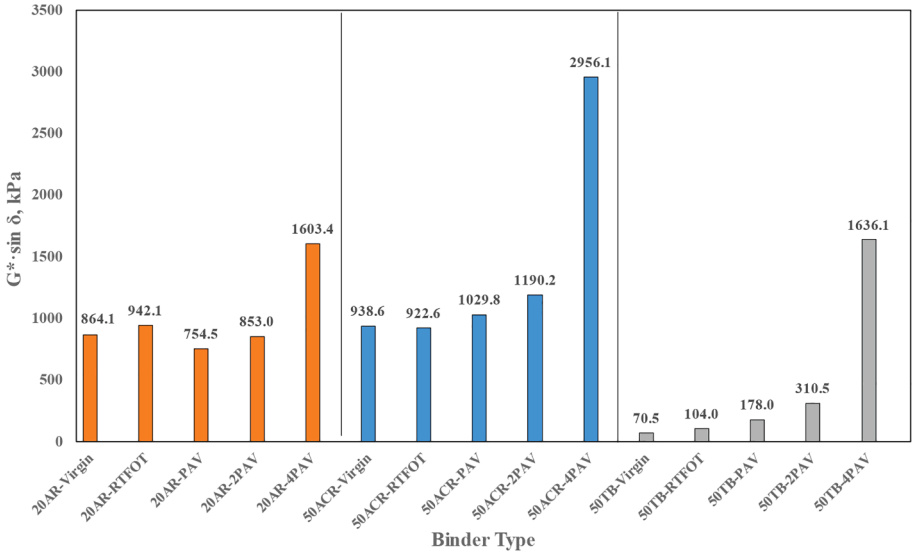

Fig. 18. Fatigue factor results of 20AR, 50ACR, and 50 TB.

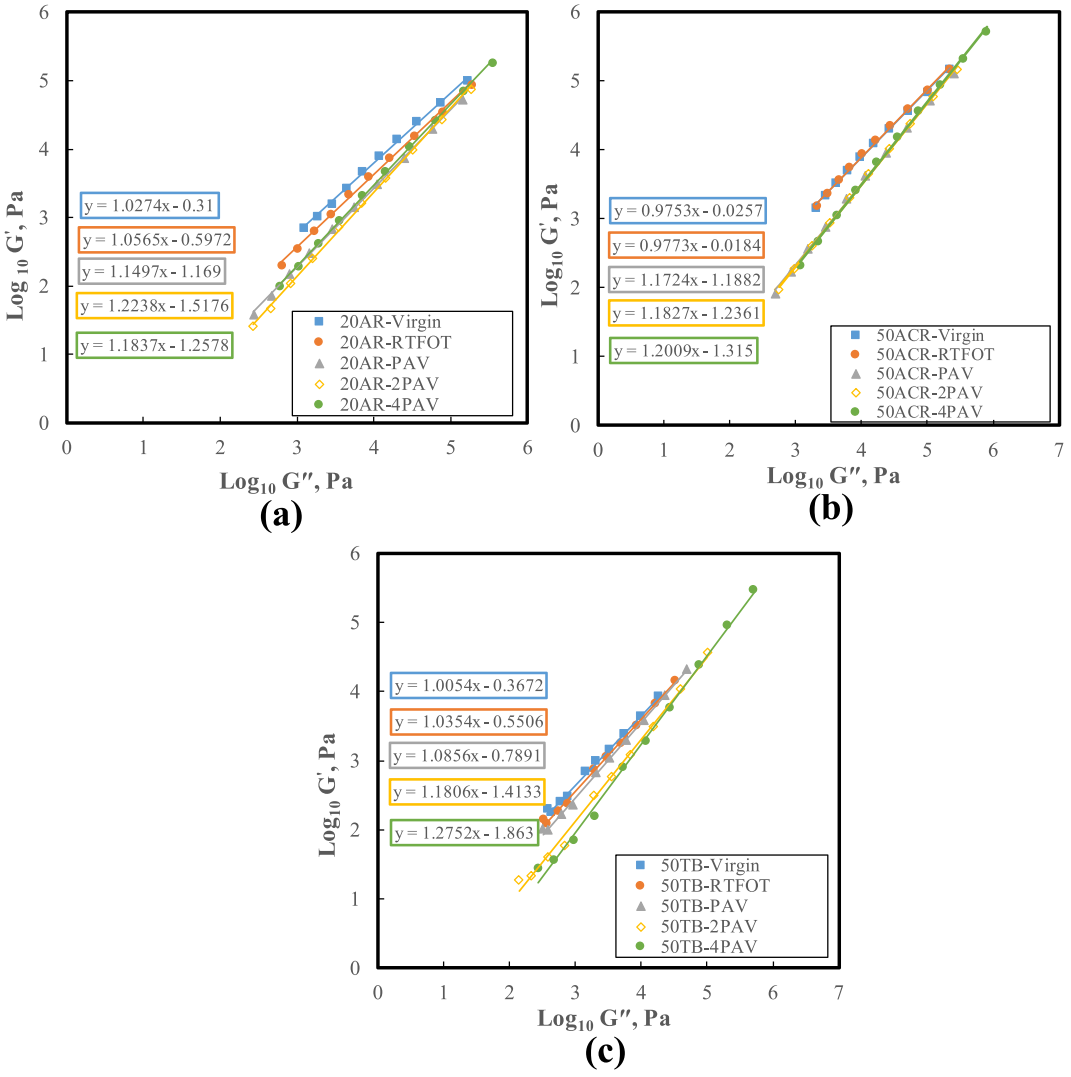

Fig. 19. Han curves of 20AR, 50ACR, and 50 TB calculated from TS test: (a) 20AR, (b) 50ACR, (c) 50 TB.

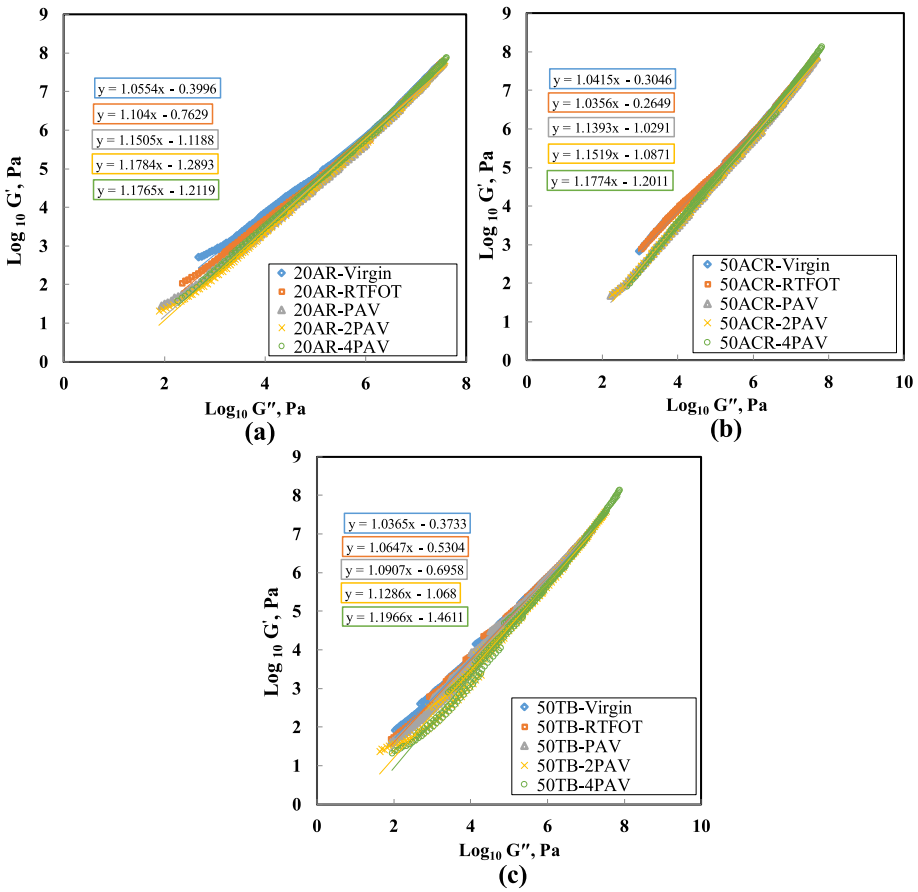

Fig. 20. Han curves of 20AR, 50ACR, and 50 TB calculated from frequency sweep test: (a) 20AR, (b) 50ACR, (c) 50 TB.

Table 6
The Han curves slopes of 20AR, 50ACR, and 50 TB calculated from the TS test.

Sample Name	Slope value				
	Virgin	RTFOT	PAV	2PAV	4PAV
20AR	1.027	1.0565	1.1497	1.2238	1.1837
50ACR	0.9753	0.9773	1.1724	1.1827	1.2009
50 TB	1.0054	1.0354	1.0856	1.1806	1.2752

Table 7
The Han curves slopes of 20AR, 50ACR, and 50 TB calculated from frequency sweep test.

Sample Name	Slope value				
	Virgin	RTFOT	PAV	2PAV	4PAV
20AR	1.0554	1.104	1.1505	1.1784	1.1765
50ACR	1.0415	1.0356	1.1393	1.1519	1.1774
50 TB	1.0365	1.0647	1.0907	1.1286	1.1996

3.7.2. *Fatigue factor*

The G*·sin δ represents the energy loss of asphalt during deformation. A smaller G*·sin δ value indicates better fatigue resistance [50]. G*·sin δ of 20AR, 50ACR, and 50 TB are shown in Fig. 18. The G*·sin δ values of 20AR, 50ACR, and 50 TB increase from RTFOT to 4PAV. It shows that aging can deteriorate the fatigue resistance of 20AR, 50ACR, and 50 TB. The G*·sin δ of the 50 TB is lower than 20AR and 50ACR at different aging conditions, indicating 50 TB has excellent fatigue resistance.

3.8. *Han curves result analysis*

Han curve is the relationship between the logarithm of G' and the logarithm of G", which is widely used in the study of the compatibility of polymeric blends [34], and the CRMA is a typical non-homogeneous polymer blend. In this paper, the Han curve is used to analyze the compatibility of HCRMA. The Han curve slope for the asphalt is closer to 2, indicating better compatibility of the polymer-modified asphalt.

Han curves of 20AR, 50ACR, and 50 TB calculated from the TS test and frequency sweep test are presented in Fig. 19 and Fig. 20, and the corresponding Han curve slope is presented in Table 6 and Table 7. Based on Table 6 and Table 7, the Han curve slopes of 20AR, 50ACR, and 50 TB before and after aging calculated by TS test and frequency sweep are similar. The Han curves slopes of 20AR, 50ACR, and 50 TB become larger after aging, and the ranking of Han curve slopes calculated by TS test and frequency sweep at 4PAV aging condition is 20AR < 50ACR < 50 TB, indicating that the compatibility of HCRMA is improved after aging, the compatibility of HCRMA is better than that of 20AR at 4PAV aging condition.

4. Conclusions

In this research, the aging performance of HCRMA with different preparation methods was investigated. Relevant properties of HCRMA such as chemical properties, rutting resistance, anti-aging properties, rheological properties, low temperature performance, fatigue resistance, and compatibility were systematically studied. The main conclusions were drawn as following:

- ATR-FTIR observations show that the I_{CA} is more recommended as a chemical index to judge the oxidation degree of HCRMA compared

with I_{SU}. In addition, $I_{S\text{-}C}$ and $I_{Si\text{-}O\text{-}Si}$ are more recommended than I_{PB} as chemical indicators for judging the degree of HCRMA desulphurization. As the aging progresses, the CR continues to undergo desulphurization and degradation reactions in the HCRMA, with the release of substances such as silica and S-C bonded material from the CR into the bituminous phase.

- The 20AR is less resistant to rutting than the 50ACR, and the 50 TB has the lowest rutting resistance. The elasticity of HCRMA decreases and then increases as the degree of aging increases. Besides, 20AR has better anti-aging properties than 50 TB and 50ACR through rheological aging index evaluation.
- The low temperature properties of HCRMA are controlled by the S value, and the low temperature stress relaxation properties of 50 TB in the PAV aging process are better than that of 20AR and 50ACR.
- Aging can reduce the integrity and fatigue resistance of HCRMA while increasing the compatibility of HCRMA. Compared with 20AR and 50ACR, 50 TB has excellent fatigue resistance, and the compatibility of HCRMA is better than that of 20AR at the 4PAV aging condition.

CRediT authorship contribution statement

Sheng Wang: Investigation, Methodology, Writing – original draft. **Weidong Huang:** Resources, Conceptualization. **Xueyan Liu:** Supervision, Writing – review & editing. **Peng Lin:** Conceptualization, Writing – review & editing.

Declaration of Competing Interest

The authors declare that they have no known competing financial interests or personal relationships that could have appeared to influence the work reported in this paper.

Acknowledgments

The authors would like to appreciate the financial support from the National Natural Science Foundation of China under Grant number 51978518. Also, the first author acknowledges the financial support from the China Scholarship Council (CSC No. 202106260114).

References

[1] J. Huang, Q.A. Wang, Influence of crumb rubber particle sizes on rutting, low temperature cracking, fracture, and bond strength properties of asphalt binder, Mater. Struct. Constr. 54 (2021) 1–15, https://doi.org/10.1617/s11527-021-01647-4.
[2] L. Cao, C. Yang, A. Li, P. Wang, Y. Zhang, Z. Dong, Flue gas composition of waste rubber modified asphalt (WRMA) and effect of deodorants on hazardous constituents and WRMA, J. Hazard. Mater. 403 (2021), https://doi.org/10.1016/j.jhazmat.2020.123814.
[3] H. Liu, Z. Zhang, Z. Li, N. Li, Effects of polyphosphoric acid (PPA), styrene-butadiene-styrene (SBS), or rock asphalt on the performance of desulfurized rubber modified asphalt, J. Appl. Polym. Sci. 138 (2021) 1–21, https://doi.org/10.1002/app.50621.
[4] H. Duan, C. Zhu, Y. Li, H. Zhang, S. Zhang, F. Xiao, S. Amirkhanian, Effect of crumb rubber percentages and bitumen sources on high-temperature rheological properties of less smell crumb rubber modified bitumen, Constr. Build. Mater. 277 (2021), 122248, https://doi.org/10.1016/j.conbuildmat.2021.122248.
[5] S.F. Kabir, R. Zheng, A.G. Delgado, E.H. Fini, Use of microbially desulfurized rubber to produce sustainable rubberized bitumen, Resour. Conserv. Recycl. 164 (2021), 105144, https://doi.org/10.1016/j.resconrec.2020.105144.
[6] L. Yin, X. Yang, A. Shen, H. Wu, Z. Lyu, B. Li, Mechanical properties and reaction mechanism of microwave-activated crumb rubber-modified asphalt before and after thermal aging, Constr. Build. Mater. 267 (2021), 120773, https://doi.org/10.1016/j.conbuildmat.2020.120773.
[7] A. Hemida, M. Abdelrahman, Component analysis of bio-asphalt binder using crumb rubber modifier and guayule resin as an innovative asphalt replacer, Resour. Conserv. Recycl. 169 (2021), 105486, https://doi.org/10.1016/j.resconrec.2021.105486.
[8] J. Huang, J. Zhang, J. Ren, H. Chen, Anti-rutting performance of the damping asphalt mixtures (DAMs) made with a high content of asphalt rubber (AR), Constr. Build. Mater. 271 (2021), 121878, https://doi.org/10.1016/j.conbuildmat.2020.121878.
[9] R. Gómez-Hernández, Y. Panecatl-Bernal, M.Á. Méndez-Rojas, High yield and simple one-step production of carbon black nanoparticles from waste tires, Heliyon. 5 (2019), https://doi.org/10.1016/j.heliyon.2019.e02139.
[10] J. Shen, B. Li, Z. Xie, Interaction between crumb rubber modifier (CRM) and asphalt binder in dry process, Constr. Build. Mater. 149 (2017) 202–206, https://doi.org/10.1016/j.conbuildmat.2017.04.191.
[11] L. Han, M. Zheng, C. Wang, Current status and development of terminal blend tyre rubber modified asphalt, Constr. Build. Mater. 128 (2016) 399–409, https://doi.org/10.1016/j.conbuildmat.2016.10.080.
[12] M. Xu, J. Liu, W. Li, W. Duan, Novel Method to Prepare Activated Crumb Rubber Used for Synthesis of Activated Crumb Rubber Modified Asphalt, J. Mater. Civ. Eng. 27 (2015) 04014173, https://doi.org/10.1061/(asce)mt.1943-5533.0001115.
[13] I.M. Ibrahim, E.S. Fathy, M. El-Shafie, M.Y. Elnaggar, Impact of incorporated gamma irradiated crumb rubber on the short-term aging resistance and rheological properties of asphalt binder, Constr. Build. Mater. 81 (2015) 42–46, https://doi.org/10.1016/j.conbuildmat.2015.01.015.
[14] M.A. Mull, K. Stuart, A. Yehia, Fracture resistance characterization of chemically modified crumb rubber asphalt pavement, J. Mater. Sci. 37 (2002) 557–566, https://doi.org/10.1023/A:1013721708572.
[15] G. Cheng, B. Shen, J. Zhang, A study on the performance and storage stability of crumb rubber-modified asphalts, Pet. Sci. Technol. 29 (2) (2011) 192–200, https://doi.org/10.1080/10916460903070421.
[16] E.I. Szerb, I. Nicotera, B. Teltayev, R. Vaiana, C.O. Rossi, Highly stable surfactant-crumb rubber-modified bitumen: NMR and rheological investigation, Road Mater. Pavement Des. 19 (5) (2018) 1192–1202, https://doi.org/10.1080/14680629.2017.1289975.
[17] S. Wang, W. Huang, Investigation of aging behavior of terminal blend rubberized asphalt with SBS polymer, Constr. Build. Mater. 267 (2021), 120870, https://doi.org/10.1016/j.conbuildmat.2020.120870.
[18] S. Wang, W. Huang, P. Lin, Low temperature and fatigue characteristics of degraded crumb rubber modified bitumen before and after aging, J. Mater. Civ. Eng. (2021), https://doi.org/10.1061/(ASCE)MT.1943-5533.0004131.
[19] J. Zhang, W. Huang, Y. Zhang, C. Yan, Q. Lv, W. Guan, Evaluation of the terminal blend crumb rubber / SBS composite modified asphalt, Constr. Build. Mater. 278 (2021), 122377, https://doi.org/10.1016/j.conbuildmat.2021.122377.
[20] S. Wang, W. Huang, P. Lin, Z. Wu, C. Kou, B. Wu, Chemical, Physical, and Rheological Evaluation of Aging Behaviors of Terminal Blend Rubberized Asphalt Binder, J. Mater. Civ. Eng. 33 (2021) 04021302, https://doi.org/10.1061/(ASCE)MT.1943-5533.0003931.
[21] G. Wang, X. Wang, S. Lv, L. Qin, X. Peng, Laboratory Investigation of Rubberized Asphalt Using High-Content Rubber Powder, Materials (Basel). 13 (2020) 4437, https://doi.org/10.3390/ma13194437.
[22] S.A. Tahami, A.F. Mirhosseini, S. Dessouky, H. Mork, A. Kavussi, The use of high content of fine crumb rubber in asphalt mixes using dry process, Constr. Build. Mater. 222 (2019) 643–653, https://doi.org/10.1016/j.conbuildmat.2019.06.180.
[23] D. Lo Presti, M.A. Izquierdo, A. Jiménez del Barco Carrión, Towards storage-stable high-content recycled tyre rubber modified bitumen, Constr. Build. Mater. 172 (2018) 106–111, https://doi.org/10.1016/j.conbuildmat.2018.03.226.
[24] M. Li, L. Liu, C. Xing, L. Liu, H. Wang, Influence of rejuvenator preheating temperature and recycled mixture's curing time on performance of hot recycled mixtures, Constr. Build. Mater. 295 (2021), 123616, https://doi.org/10.1016/j.conbuildmat.2021.123616.
[25] L. Liu, M. Li, Q. Lu, Two-Step Mixing Process Elaboration of the Hot-Mix Asphalt Mixture Based on Surface Energy Theory, J. Mater. Civ. Eng. 32 (2020) 04020301, https://doi.org/10.1061/(ASCE)MT.1943-5533.0003400.
[26] M. Zadshir, D. Ploger, X. Yu, C. Sangiorgi, H. Yin, Chemical, thermophysical, rheological, and microscopic characterisation of rubber modified asphalt binder exposed to UV radiation, Road Mater. Pavement Des. 21 (2020) S123–S139, https://doi.org/10.1080/14680629.2020.1736606.
[27] A.V. Kataware, D. Singh, Effect of short-term ageing on high-temperature performance of SBS modified binder containing warm mix asphalt additives, Road Mater. Pavement Des. 21 (3) (2020) 623–642, https://doi.org/10.1080/14680629.2018.1509804.
[28] B. Fethiza Ali, K. Soudani, S. Haddadi, Effect of waste plastic and crumb rubber on the thermal oxidative aging of modified bitumen, Road Mater. Pavement Des. (2020) 1–12, https://doi.org/10.1080/14680629.2020.1820893.
[29] AASHTO M 320-14. Standard Specification for Performance-Graded Asphalt Binder, Washington, D.C., 2014.
[30] S. Wang, W. Huang, A. Kang, Evaluation of Aging Characteristics of High-Viscosity Asphalt: Rheological Properties, Rutting Resistance, Temperature Sensitivity, Homogeneity, and Chemical Composition, J. Mater. Civ. Eng. 33 (2021) 04021149, https://doi.org/10.1061/(ASCE)MT.1943-5533.0003777.
[31] S. Wang, W. Huang, Q. Lv, C. Yan, P. Lin, M. Zheng, Influence of different high viscosity modifiers on the aging behaviors of SBSMA, Constr. Build. Mater. 253 (2020), 119214, https://doi.org/10.1016/j.conbuildmat.2020.119214.
[32] N. Tang, W. Huang, F. Xiao, Chemical and rheological investigation of high-cured crumb rubber-modified asphalt, Constr. Build. Mater. 123 (2016) 847–854, https://doi.org/10.1016/j.conbuildmat.2016.07.131.
[33] P. Lin, C. Yan, W. Huang, Y. Li, L. Zhou, N. Tang, F. Xiao, Y. Zhang, Q. Lv, Rheological, chemical and aging characteristics of high content polymer modified asphalt, Constr. Build. Mater. 207 (2019) 616–629, https://doi.org/10.1016/j.conbuildmat.2019.02.086.

[34] C.D. Han, J.K. Kim, Molecular theory for the viscoelasticity of compatible polymer mixtures. 1. A tube model approach, Macromolecules. 22 (4) (1989) 1914–1921, https://doi.org/10.1021/ma00194a067.
[35] AASHTO M 332-14. Standard Specification for Performance-Graded Asphalt Binder using Multiple Stress Creep Recovery (MSCR) Test, Washington, D.C., 2014.
[36] ASTM D6648. Standard test method for determining the flexural creep stiffness of asphalt binder using the bending beam rheometer (BBR), West Conshohocken, PA, 2001.
[37] P. Lin, W. Huang, N. Tang, F. Xiao, Y. Li, Understanding the low temperature properties of Terminal Blend hybrid asphalt through chemical and thermal analysis methods, Constr. Build. Mater. 169 (2018) 543–552, https://doi.org/10.1016/j.conbuildmat.2018.02.060.
[38] P. Lin, W. Huang, Y. Li, N. Tang, F. Xiao, Investigation of influence factors on low temperature properties of SBS modified asphalt, Constr. Build. Mater. 154 (2017) 609–622, https://doi.org/10.1016/j.conbuildmat.2017.06.118.
[39] AASHTO TP101, Standard Method of Test for Estimating Damage Tolerance of Asphalt Binders Using the Linear Amplitude Sweep., Washington, DC, 2012.
[40] F. Safaei, C. Castorena, Temperature effects of linear amplitude sweep testing and analysis, Transp. Res. Rec. 2574 (1) (2016) 92–100, https://doi.org/10.3141/2574-10.
[41] F. Safaei, C. Castorena, Material nonlinearity in asphalt binder fatigue testing and analysis, Mater. Des. 133 (2017) 376–389, https://doi.org/10.1016/j.matdes.2017.08.010.
[42] F. Safaei, C. Castorena, Y.R. Kim, Linking asphalt binder fatigue to asphalt mixture fatigue performance using viscoelastic continuum damage modeling, Mech. Time-Dependent Mater. 20 (3) (2016) 299–323, https://doi.org/10.1007/s11043-016-9304-1.
[43] J.A. D'Angelo, The Relationship of the MSCR Test to Rutting, Road Mater. Pavement Des. 10 (sup1) (2009) 61–80.
[44] D.A. Anderson, Y.M. Le Hir, J.-P. Planche, D. Martin, A. Shenoy, Zero shear viscosity of asphalt binders, Transp. Res. Rec. 1810 (1) (2002) 54–62.
[45] A. Behl, S. Chandra, V.K. Aggarwal, S. Gangopadhyay, Zero shear viscosity of bitumen-filler mastics of warm-mix binders, J. Mater. Civ. Eng. 27 (2015), https://doi.org/10.1061/(ASCE)MT.1943-5533.0001232.
[46] S. Wang, W. Huang, A. Kang, Laboratory evaluation of the properties of high-cured crumb rubber modified asphalt containing sulfur and polymer after the oxidative aging procedure, Constr. Build. Mater. 304 (2021), 124611, https://doi.org/10.1016/j.conbuildmat.2021.124611.
[47] C. Riccardi, A. Cannone Falchetto, D.i. Wang, M.P. Wistuba, Effect of cooling medium on low-temperature properties of asphalt binder, Road Mater. Pavement Des. 18 (sup4) (2017) 234–255, https://doi.org/10.1080/14680629.2017.1389072.
[48] D. Wang, A.C. Falchetto, C. Riccardi, L. Poulikakos, B. Hofko, L. Porot, M. P. Wistuba, H. Baaj, P. Mikhailenko, K.H. Moon, Investigation on the combined effect of aging temperatures and cooling medium on rheological properties of asphalt binder based on DSR and BBR, Road Mater. Pavement Des. 20 (2019) S409–S433, https://doi.org/10.1080/14680629.2019.1589559.
[49] Q. Li, G. Sun, Y. Lu, Y. Meng, S. Luo, L. Gao, Effects of warm-mix asphalt technologies and modifiers on pavement performance of recycled asphalt binders, J. Clean. Prod. 282 (2021), 125435, https://doi.org/10.1016/j.jclepro.2020.125435.
[50] X. Yu, Y. Wang, Y. Luo, Impacts of water content on rheological properties and performance-related behaviors of foamed warm-mix asphalt, Constr. Build. Mater. 48 (2013) 203–209, https://doi.org/10.1016/j.conbuildmat.2013.06.018.